# THERMOMECHANICAL MODELING OF NITI SHAPE MEMORY ALLOYS INCLUDING PLASTICITY

A THESIS SUBMITTED TO
THE GRADUATE SCHOOL OF NATURAL AND APPLIED SCIENCES
OF
MIDDLE EAST TECHNICAL UNIVERSITY

BY

HAMDI ALPAY KÜÇÜKER

IN PARTIAL FULFILLMENT OF THE REQUIREMENTS
FOR
THE DEGREE OF MASTER OF SCIENCE
IN
MECHANICAL ENGINEERING

AUGUST 2022

Approval of the thesis:

**THERMOMECHANICAL MODELING OF NITI SHAPE MEMORY ALLOYS INCLUDING PLASTICITY**

submitted by **HAMDI ALPAY KÜÇÜKER** in partial fulfillment of the requirements for the degree of **Master of Science in Mechanical Engineering Department, Middle East Technical University** by,

Prof. Dr. Halil Kalıpçılar
Dean, Graduate School of **Natural and Applied Sciences** _____

Prof. Dr. Sahir Arıkan
Head of Department, **Mechanical Engineering** _____

Prof. Dr. Haluk Darendeliler
Supervisor, **Mechanical Engineering, METU** _____

Prof. Dr. Günay Anlaş
Co-supervisor, **Mechanical Engineering, Boğaziçi University** _____

**Examining Committee Members:**

Prof. Dr. Suat Kadıoğlu
Mechanical Engineering, METU _____

Prof. Dr. Haluk Darendeliler
Mechanical Engineering, METU _____

Prof. Dr. Serkan Dağ
Mechanical Engineering, METU _____

Assoc. Prof. Dr. Hüsnü Dal
Mechanical Engineering, METU _____

Prof. Dr. Can Çoğun
Mechatronics Engineering, Çankaya University _____

Date:

**I hereby declare that all information in this document has been obtained and presented in accordance with academic rules and ethical conduct. I also declare that, as required by these rules and conduct, I have fully cited and referenced all material and results that are not original to this work.**

Name, Surname: Hamdi Alpay Küçüker

Signature :

# ABSTRACT

## THERMOMECHANICAL MODELING OF NITI SHAPE MEMORY ALLOYS INCLUDING PLASTICITY

Küçüker, Hamdi Alpay
M.S., Department of Mechanical Engineering
Supervisor: Prof. Dr. Haluk Darendeliler
Co-Supervisor: Prof. Dr. Günay Anlaş

August 2022, 58 pages

Shape memory alloys (SMA) are unique materials with an ability to recover their original shape from large deformations when unloaded and/or subjected to heat. Their ability to recover from large strains, due to martensitic transformation, even under excessive loading allows them to be used in various different sectors including aerospace, biomedical and automotive. The present thesis summarizes the studies on constitutive modelling of SMAs and the effect of plasticity on it. Based on the experiments and tests presented in the literature, an already existing 3D constitutive model is modified in order to include the effect of plastic strain.

The model used in this thesis, includes the conventional characteristic behaviour of SMA, namely two way shape memory effect (TWSME) and superelasticity, as well as the plastic strain. The generated constitutive model is implemented into finite element tool via a user subroutine code. The model can capture the strains caused from both transformation and plastic deformation. The model is applied to the analysis of a spring in tension, simple tension test and a three point bending test.

The proposed plasticity modified constitutive model predicted the behaviour of the SMA and showed similar results with the experimental data available in the literature.

Keywords: Shape Memory Alloys, Plasticity, Martensitic Transformation, Constitutive Equation, Modelling

# ÖZ

## NİTİ ŞEKİL HAFIZALI ALAŞIMLARIN PLASTİSİTE İLE TERMOMEKANİK MODELLENMESİ

Küçüker, Hamdi Alpay
Yüksek Lisans, Makina Mühendisliği Bölümü
Tez Yöneticisi: Prof. Dr. Haluk Darendeliler
Ortak Tez Yöneticisi: Prof. Dr. Günay Anlaş

Ağustos 2022 , 58 sayfa

Şekil hafızalı alaşımlar, üzerindeki yük kaldırılınca ve/veya ısıtılınca, uğradığı büyük deformasyonlara rağmen ilk şeklini geri kazanabilme özelliğine sahip malzemelerdir. Şekil hafızalı alaşımların yüksek yüklemeler altında bile martenzitik dönüşüm sayesinde büyük gerinimlerin geri dönüşümünü sağlayabilmesi, havacılık, biyomedikal ve otomotiv gibi pek çok sektörde kullanımına yol açmıştır. Bu tezde şekil hafızalı alaşımların bünye modelleri üzerine yapılan son çalışmalar ve plastisitenin etkisi anlatılmıştır. Literatürde yapılmış olan test ve deneylere dayanarak mevcut bir üç boyutlu bünye modeli plastik gerinimi de içerecek şekilde değiştirilmiştir.

Bu tezde kullanılan bünye modeli şekil hafızalı alaşımların yaygın özellikleri olan, iki yönlü şekil hafıza etkisi (İYŞHE) ve süperelastisitenin yanı sıra plastik gerinim oluşumunu da içermektedir. Elde edilen bünye modeli bir kullanıcı alt programı ile sonlu elemanlar yazılımına eklenmiştir. Model dönüşüm ve plastisite nedeniyle oluşan gerinimleri hesaplayabilmektedir. Uyarlanan model ile gerilmiş bir yay, basit gerilme deneyi ve üç nokta eğme deneyi analiz edilmiştir.

Önerilen bünye modeli, literatürde olan deneysel çalışmalar ile uyumlu olacak şekilde sonuç vermiştir.

Anahtar Kelimeler: Şekil Hafızalı Alaşımlar, Plastisite, Martenzitik Dönüşüm, Konstitütif Denklem, Modelleme

To my family and friends

## ACKNOWLEDGMENTS

I would like to express my thanks and pay my respects to my Thesis Supervisor Prof. Dr. Haluk Darendeliler for his support and endless help and to my Co-Supervisor Prof. Dr. Günay Anlaş for his valuable contributions and supports throughout the preparation of this thesis.

I would like to thank my darling Cansu Güneş for her love, trust and support. She is the one who encouraged me to continue my graduate education while going through tough times. Her patience, care and selfless love during the process, made everything easier for me. Writing this thesis and graduating would not be possible without her.

I would like to express my thanks and regards to my family, my father Mehmet C. Küçüker, my mother Esin Küçüker, my brother K. Alper Küçüker, my sister Merve Küçüker, my grandfather Hamdi Kucur, my grandmother Sabahat Kucur, my uncle Erol Kucur and to all of my family members whom I can not mention here. They are the ones who broadened my horizon, showed me how to be a better person and supported me in every moment and every aspect of my life. I feel so grateful to be surrounded by such a loving family who have always faith in me.

I would like to thank my friends and colleagues at TAI. They are the ones who tolerated me and showed me support during my graduate education. Thanks to their help and understanding, everything was easier than it would be.

## TABLE OF CONTENTS

# LIST OF TABLES

TABLES

## LIST OF FIGURES

FIGURES

## LIST OF ABBREVIATIONS

| | |
|---|---|
| SMA | Shape Memory Alloy |
| $M_s$ | Martensite Start Temperature |
| $M_f$ | Martensite Finish Temperature |
| $A_s$ | Austenite Start Temperature |
| $A_f$ | Austenite Finish Temperature |
| SME | Shape Memory Effect |
| $A_s$ | Austenite Start Temperature |
| $\sigma_s$ | Detwinning Start Stress |
| $\sigma_f$ | Detwinning Finish Stress |
| OWSME | One Way Shape Memory Effect |
| TWSME | Two Way Shape Memory Effect |
| TRIP | Transformation Induced Plasticity |
| $C_A$ | Austenite Stress Influence Coefficient |
| $C_M$ | Martensite Stress Influence Coefficient |
| $\dot{E}$ | Total Energy Rate |
| $\dot{W}$ | Rate of Work Done By External Forces |
| $\dot{Q}$ | Rate of Heat Energy |
| $\dot{K}$ | Kinetic Energy Rate |
| $\dot{U}$ | Internal Energy Rate |
| $V$ | Volume |
| $S$ | Surface |
| $r$ | Heat Source |
| $q$ | Heat Flux |
| $u$ | Specific Internal Energy |

| | |
|---|---|
| $t_{(n)}$ | Traction per Unit Area |
| $b$ | Body Force |
| $v$ | Velocity Field |
| $\rho$ | Density |
| $\sigma$ | Stress |
| $D$ | Deformation Rate Tensor |
| $s$ | Entropy |
| $T$ | Temperature |
| $u$ | Internal Energy |
| $h$ | Enthalpy |
| $\Psi$ | Helmholtz Free Energy |
| $G$ | Gibbs Free Energy |
| $\epsilon$ | Strain |
| $\xi$ | Martensitic Volume Fraction |
| $S$ | Compliance Tensor |
| $\alpha$ | Thermal Expansion Tensor |
| $c$ | Effective Specific Heat |
| $s_0$ | Effective Specific Entropy |
| $u_0$ | Effective Specific Internal Energy |
| $\Lambda^t$ | Transformation Tensor |
| $H$ | Transformation Tensor Variable |
| $\sigma'$ | Deviatoric Stress |
| $\bar{\sigma'}$ | Equivalent Deviatoric Stress |
| $\pi^t$ | Thermodynamic Force |
| $\Phi^t$ | Transformation Function |
| $f^t$ | Transformation Hardening Function |
| $\epsilon^p$ | Plastic Strain |

| | |
|---|---|
| $\beta$ | Backstress |
| $\bar{\epsilon^p}$ | Equivalent Plastic Strain |
| $\Lambda^p$ | Plastic Strain Tensor |
| $\pi^p$ | Thermodynamic Force for Plasticity |
| $\Phi^p$ | Plasticity Function |
| $f^p$ | Plastic Hardening Function |
| $Y_0$ | Initial Yield Stress |
| $Y_m$ | Plastic Yield Plateau |
| $K_\beta$ | Kinematic Hardening Modulus |
| $C_H$ | Hardening Constant |
| $R_t$ | Transformation Strain Residual |
| $R_p$ | Plastic Strain Residual |

# CHAPTER 1

# INTRODUCTION

Metals have been reliable and commonly used materials in terms of structural application. From the beginning of the earlier ages, strengthening metals by using different manufacturing techniques was used by mankind. As the metallurgical science has improved, understanding of material nature and behaviour within certain conditions, has upgraded considerably. In last few decades, the enhancement in material engineering led to evolution of new alloys and composite materials with far more different and unique properties than ordinary metals. This kind of materials, with lower density, strong material properties and additional engineering functions are gathered under a new group called, *multifunctional materials*. The multifunctional materials that has the ability of sensing and actuation is known as *active materials*. [1]

In general, active materials have the capability of mechanical response, when they are exposed to non-mechanical loads such as thermal, magnetic and electrical. Piezoelectric ceramics, magnetostrictive ceramics, ionic electroactive polymers, shape memory polymers and shape memory alloys can be given as examples of active materials. In this study, shape memory alloys will be investigated.

## 1.1 Background

*Shape Memory Alloys* are, as the name suggests, unique materials with the ability of shape recovery when subjected to heat. Due to their excessive actuation energy, shape memory alloys can restore their initial shape, although they are being exposed to heavy loading. This actuation energy capacity leads Shape Memory Alloys (SMA) to be used in numerous different sectors including aerospace, biomedical etc. Some

examples are shown in figure 1.1

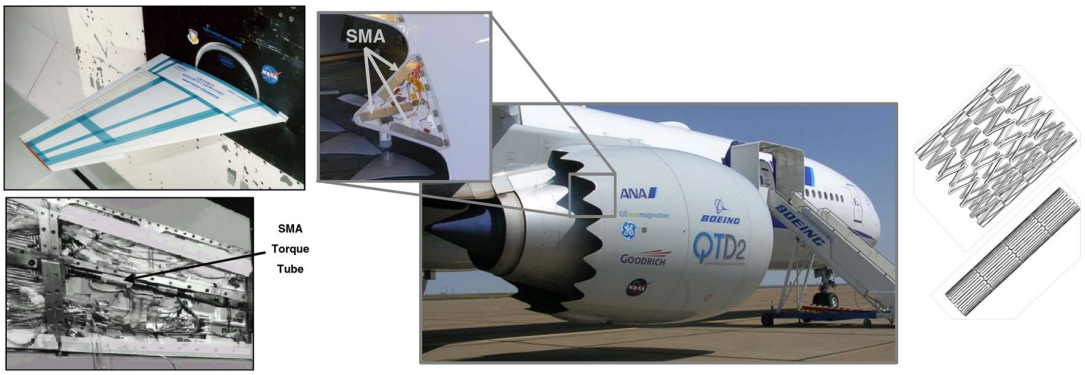


Figure 1.1: Some examples of Shape Memory Alloys in different applications. SMA torque tube in an aircraft actuation system (Left). Self-expanding stant for medical applications (Right). Active chevron structure of an aircraft (Middle) [1]

SMAs have two distinct phases, *austenite* and *martensite*.These phases have separate mechanical properties and crystalographic structure. In general, austenite has a cubical crystal structure while martensite may be tetragonal. The main reason of shift between the phases is shear lattice distortion, which named as *Martensitic Transformation*. Martensitic crystal form orientations may differ in direction, this variation of direction is called *variant*. Martensitic variant assembly may consist of two forms; twinned martensite and detwinned martensite. The phase transformation between austenite, twinned martensite and detwinned martensite results in the uncommon characteristic of SMA.

The phase transition from austenite to martensite, by cooling, called as *forward transformation*. In reverse, upon heating, martensite phase shifts to austenite phase resulting in *reverse transformation*. When an SMA in austenite phase is cooled down, the material starts to transform to martensite at *Martensite Start Temperature,* $M_s$ and transforms completely to martensite when the temperature reaches *Martensite Finish Temperature,* $M_f$. Similarly, when the material is in a fully martensitic state and heated up, it starts to transform to austenite at *Austenite Start Temperature,* $A_s$ and transforms completely to austenite at *Austenite Finish Temperature,* $A_f$. Transformation temperatures tend to change with the introduction of stress. The schematic of the forward and reverse tranformation of SMAs is shown in Figure 1.2.

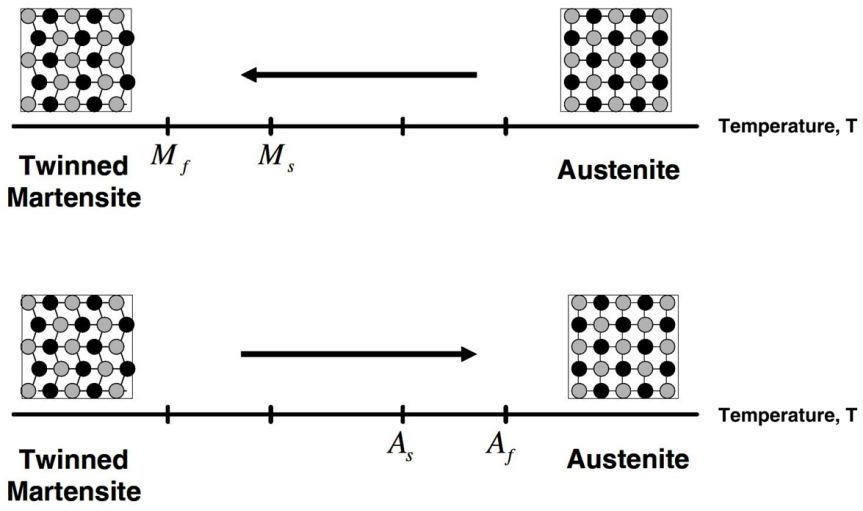


Figure 1.2: Forward and Reverse Transformation [1]

If a mechanical load is applied to SMAs at martensitic phase, the load may cause the reorientation of variants resulting in detwinning, which is also the cause of an irrecoverable macroscopic deformation, even if the loading is released. At this stage, if the material is heated up above $A_f$, the material will undergo phase transformation and complete shape recovery. The material will keep its recovered shape even though it is cooled down to a temperature lower than $M_f$. This behaviour of the SMAs is called the *Shape Memory Effect (SME)*. Similar to temperature labeling, the minimum stress required to detwinning initiation is *Detwinning Start Stress,* $\sigma_s$ and the stress required for detwinning completion is *Detwinning Finish Stress,* $\sigma_f$ If a material in austenite phase is cooled down to below $M_f$ temperature, while being subjected to stress above $\sigma_f$, the material transforms directly to detwinned martensite from austenite, resulting in a shape change. Figure 1.3 shows the combination of forward and reverse transformation along with detwinning.

In addition to thermal loading, SMAs can also undergo phase transformation with mechanical loading only. If an initially austenite SMA with temperature above $A_f$ is subjected to a load higher than $\sigma_{Mf}$, starting from $\sigma_{Ms}$, material will begin to change its phase and the resultant phase would be detwinned martensite. Reversely, if a loaded detwinned martensite material with temperature higher than $A_f$ is relieved, SMA transforms to austenite starting from $\sigma_{As}$ until $\sigma_{Af}$ up to fully austenite. This behaviour is called *Pseudoelastic Effect* and it is as a result of stress induced trans-

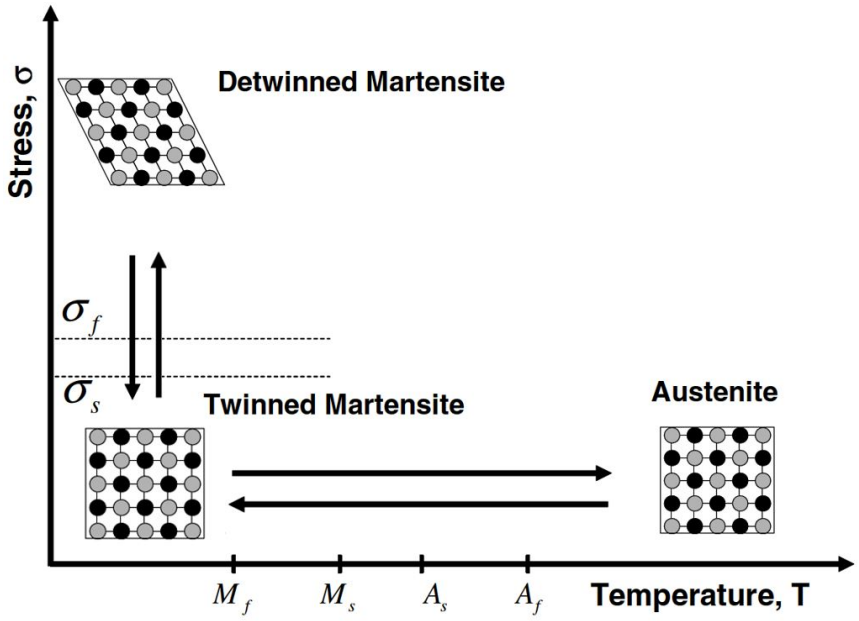


Figure 1.3: Forward, Reverse and Stress Induced Transformation [1]

formation. Pseudoelastic effect can also be referred as *Superelastic* or *Rubber-like* behaviour [5]. SME and pseudoelastic effect are the most important characteristic properties of SMAs.

Figure 1.4 shows the stress-strain-temperature relation of SMAs. Starting from austenite, following the direction indicated by arrow, SMA cooled down below $A_s$ into twinned martensite phase. With the introduction of mechanical load, detwinning occurs until the end of $\sigma_f$ concluding detwinned martensite phase of the material. Upon unloading, a residual strain, around 4% is observed. This strain is named as *Transformation strain* and it is different from conventional plastic strain.

Basically, transformation strain is a result of the shape change during detwinning process. Transformation strain, as can be seen from the Figure 1.4 can be vanished when SMA is exposed to heat and the phase switches back to austenite, as described by SME. If a SMA can only follow the direction indicated by the arrow in Figure 1.4, the SMA is labeled as to have *One Way Shape Memory Effect (OWSME)*. Otherwise, if a SMA is able to carry cyclic thermal loading in both direction. It is said to have *Two Way Shape Memory Effect (TWSME)*.

Usually, the applications of SMA requires reversibility. For example, an electrically

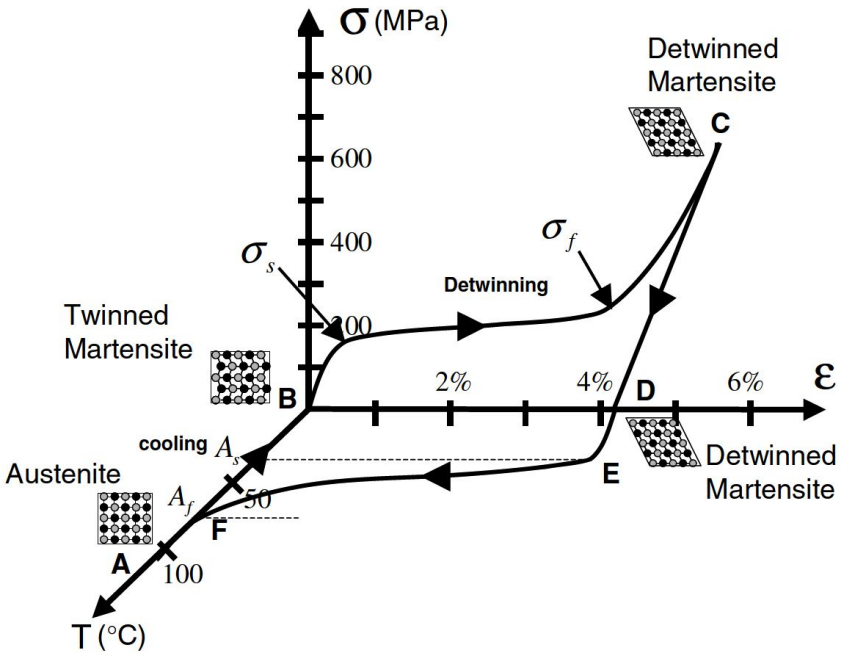


Figure 1.4: Shape Memory Effect of SMA [1]

driven actuator with SMA material inside, requires temperature increase to actuate in a certain direction, in order to preserve functionality, SMA element should return back to its original form once the thermal loading is inactive. Therefore SMA should be reversable upon various loading to be reliable. Considering the importance of reversibility, many researches have been done on the cyclic behaviour of SMAs. *Transformation Induced Plasticity, (TRIP)* is one of the most important and critical properties of SMAs. As the thermal or mechanical loading is introduced in cyclic manner, a minor residual strain can be observed at the end of each cycle. These minor residual strains as can be seen from Figure 1.5, accumulate, as the number of cycle is increased resulting in a major material property change [6]. Since TRIP has a direct affect on functionality of SMA, it is a trending reasearch area for scientists.

The material combination has a considerable affect on SMA behaviour. The most popular and commonly used shape memory alloy is based on Nickel and Titanium, and named as Niti SMA or more conventionally *Nitinol*. With the introduction of the new elements, the behaviour of the Niti SMA may also be changed. For example, addition of Cu into Niti (NiTiCu), results in hystheresis and maximum transformation strain reduction. On the other hand, adding Niobium (Nb), NiTiNb increases the hys-

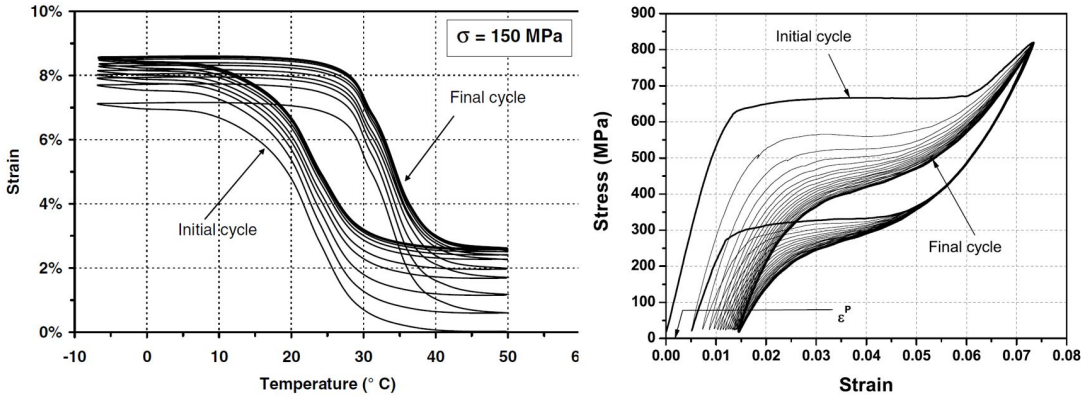


Figure 1.5: Transformation Induced Plasticity. Cyclic thermal loading under constant stress(Left). Cyclic mechanical loading under constant temperature 70 °C (Right) [1]

theresis range of SMA. Pb, Pti Hf and Zr elements can be also added into NiTi SMA in order to achieve different characteristics. In addition to NiTi alloys, coper-based and iron-based alloys shows SMA characteristic. These materials are also being used due to their low cost, high temperature resistance or better pseudoelastic behaviour.

In order to describe the behaviour of shape memory alloys and construct the constitutive equations, certain thermomechanical material properties should be defined. Excluding transformation, the thermoelastic properties of pure austenite and martensite phases should be known. These properties are required to describe the behaviour of the SMA while no transformation is occuring in both direction. The critical temperatures ($M_f$, $M_s$, $A_s$, $A_f$) and critical stress ($\sigma_s$, $\sigma_f$) values that defined in the previous pages, should also be known. Using these parameters, the transformation occurence points according to current stress and temperature can be calculated. Transformation strain evolution parameters are another one of the necessary properties. While detwinning is on, the transformation strain rate should be known. *Stress influence coefficients* or the transformation surface slopes $C_A$ and $C_M$, shown in Figure 1.6 are the parameters that is limiting SMA's phase transitions. As the figure shows the martensite and austenite start and finish temperatures may be changed with the introduction of the mechanical loading.

The rate of change of these temperature values according to stress gives the $C_A$ and $C_M$. $H_{max}$ the *Maximum Available Transformation Strain* is generally decided empirically, however the relation between stress and $H_{max}$ is another open research area.

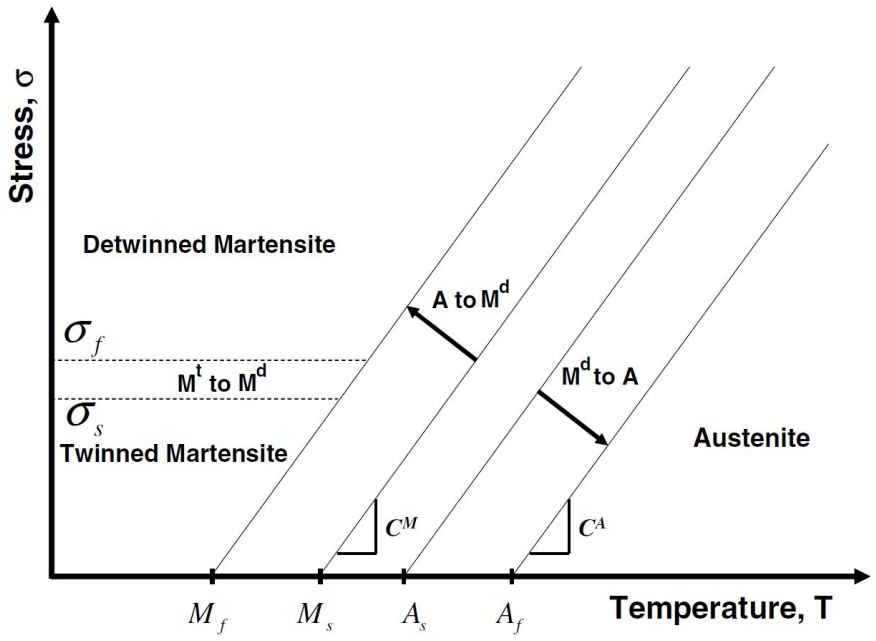


Figure 1.6: Stress Influence Coefficients, $C_A$ and $C_M$ [1]

The transformation of material phase from austenite to martensite and martensite to austenite, in other words forward and reverse transformation, is related to release and absorb of latent heat [7]. The heat disturbance during the transformation and transformation temperatures are usually obtained using *Differential Scanning Calorimeter (DSC)*. The DSC is a very common thermal analysis method. With the introduction of a very few material specimen, DSC can be used to obtain, transformation temperatures, the latent heat during the transformation, the specific heat of the different material phases [8].

The working principle of DSC depends on the heat applied to or absorbed from the system that is resulting in a constant cooling or heating rate. When a material undergo tranformation, DSC detects the instability and a disturbance is shown on the monitor indicating the transformation of the material. The start and end point of the disturbances basically decides the start and finish temperatures for both forward and reverse transformation. Figure 1.7 shows a classical thermograph result obtained from DSC during heating and cooling stages. Once the $M_f$, $M_s$, $A_s$, $A_f$ temperatures are obtained, the stress influence coefficients, $C_A$ and $C_M$ can be found by repeating the DSC test under various loading conditions.

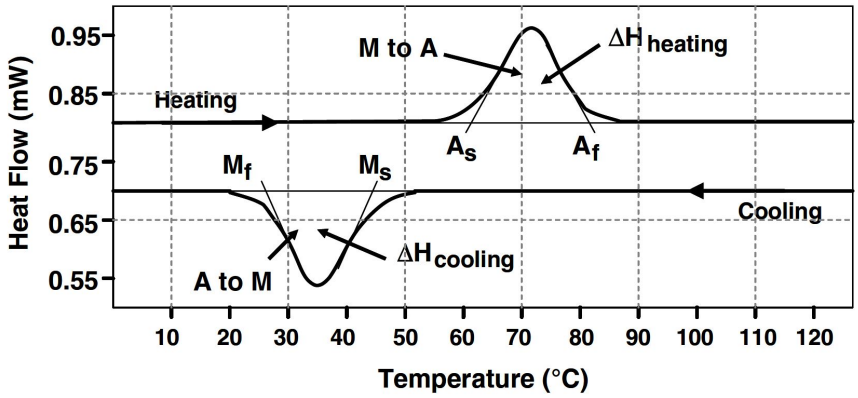


Figure 1.7: DSC Thermograph Showing the Transformation Start and Finish Temperatures [1]

Experiments in SMA generally conducted in order to obtain the characterization of material. Mechanical properties are aimed to be achieved at the end of experimental studies. In order to satisfy these needs, ASTM has standardized the test procedures which results an increase in specimen demand. In general, shape memory alloys are hard to machine with the current manufacturing techniques [1]. Due to its simplicity in geometry and relatively high tensile strength, wires are the most common test specimens in the research area. Wires, in general, easy to access and usable without any additional processes. However due to its low grip area, it is challenging to apply the force without causing a stress concentration at the grip points. Therefore, SMA wire specimen mostly requires a grip mechanism which comes with additional cost and design phases. Figure 1.8 shows an example of a test system including SMA wire and a custom grip.

There are also straps and dogbone specimens as an 2D and 3D specimen, being used in test studies. These specimen are usually manufactured by *Electrical Discharge Machining (EDM)*. Figure 1.9 shows examples for wire, 2D and 3D specimens.

## 1.2 Motivation and Problem Definition

With the exploration of SMA behaviour through experiments a need for the modelling of SMAs has risen. The studies on constitutive modelling have increased in last few

decades. In order to predict the behaviour of the SMA correctly, different approaches has been used to model the constitutive behaviour. The study of Noll, Coleman and Gurtin [9] is accepted to be the first in modelling the thermomechanical constitutive equations for SMA, using fundamental principles of continuum mechanics.

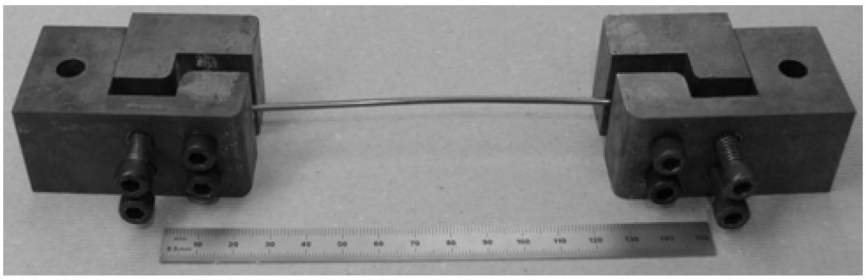

Figure 1.8: SMA Experiment, Wire Located Between Custom Grips

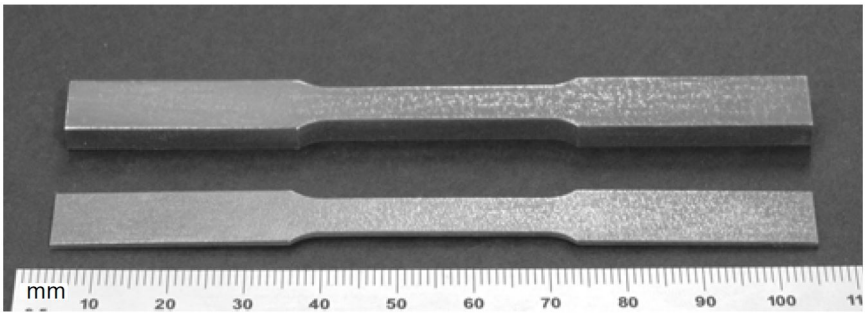


Figure 1.9: SMA 2D and 3D Dogbone Specimens

With the contribution of Lagoudas and Machado [10] and Liang and Rodgers [11], the constitutive modelling of SMA has been done using first and second law of thermodynamics with Gibbs or Helmholtz free energy respectively. Lagoudas has implemented the model into a finite element tool [12] via special material definiton. Although the numerical model can simulate the SME and superelastic behaviour of SMA in 3D structures, no effect of plasticity was included in the model. Hartl and Lagoudas [4] have extended the model so that it would cover the plastic behaviour along with unique properties of SMA.

## 1.3 Objective of the Thesis

In this thesis, a constitutive model is presented to analyze the deformation of SMAs including the plastic deformation. For this purpose, the plastic behaviour of the SMA is embeded in to the finite element code so that the material behaviour under excessive loading can be observed.

## 1.4 Scope of the Thesis

In this thesis to include the plastic deformation into the constitutive model, an open source code written by Karakalas [2] based on the model of Lagoudas and Hartl [3] is modified such that the plastic behaviour of the material is predicted under excessive loading. The same plasticity model of the Hartl and Lagoudas [4] and an alghorithm with Newton-Rhapson method by Karakalas [2] is used in order to correctly simulate the behaviour of the SMA with plasticity. The tests and experiments in the mentioned papers [4], [3] are compared with the modified code results.

## 1.5 The Outline of the Thesis

In this thesis, there are five main chapters. The Introduction chapter starts with a general information on SMAs and basically defines the SMA materials and their characteristic behaviour under different temperature and load inputs. Important parameters that are used to model the constitutive behaviour are introduced. In the literature survey chapter, from the first modelling approaches to latest contributions done in the SMA field are briefly described and their contribution to this study is outlined. In the governing equations chapter, the constitutive equations along with the algorithm description that is used in this paper are explained in detail. In the results and discussion chapter, a comparison of the proposed model with the experimental results in the literature are introduced. The similarities and differences between the experiment and proposed model results are discussed. Possible reasons of incompatibilities are investigated. Lastly, in the conclusion, the rational behind the outcomes in the previous chapter is discussed and the future study is mentioned shortly. At the end of the

chapters, referred documents are listed under the references section.

# CHAPTER 2

# LITERATURE SURVEY

Shape Memory Alloys (SMA) have been the focus of researche in the last few decades. As the demand of smart structures or multifunctional materials has increased, the investigations done on the SMA have risen significantly. SMAs has started to be considerable part of some of the industries due to its functional characteristics. Aviation, medical and transportation are the leading fields that SMAs are being used frequently. In order to use SMA in engineering application, the capabilities and limitations should be understood thoroughly. Therefore, constitutive modelling along with computational implementation in finite element tool and the experimental studies are major point of interests. This chapter is divided into two sections. Each section will cover different field of study namely, experimental studies, constitutive modelling and numerical implementation.

## 2.1 Experimental Studies

The first issued study on SMA or TiNi as it is referred in the papers at that time, has done in U.S. Naval Ordnance Laboratory in 1961 [13]. In this study, various mechanical properties including tensile strength, melting point, hardness were experimentally found and reported. Based on that study, in 1963 the shape recovery feature of the SMA was discovered and reported [14]. This finding had an outstanding effect on the field and lead to many other researches to be done. The important studies done on the SMA at Naval Ordnance Laboratory has resulted in the commonly used name of NiTi alloys, "*Nitinol*" where the suffix "*nol*" stands for the Naval Ordnance Laboratory.

Once the material was discovered, the research focus shifted to further investigation of

the crystallographic build-up. The studies on shape memory effect and superelasticity [15, 16] rose significantly in terms of metallurgy and microstructure. As the science got more familiar with the unique properties of SMA and the reactions of the material are recognized more, the usage in the industry became unavoidable. Considering the high actuation capability of SMA with low cost, it is started to be the main focus of engineering study in late twentieth century [17, 18, 19, 20, 21].

The excessive increase in the usage of SMA in engineering applications has led to necessity of testing and experiment standards. In order to meet this requirement, ASTM International published a number of standards indicating a correct and precise method to test SMAs. One of the standards [22], directly focusing the tensile test of SMA, is showing superelastic behaviour in room temperature conditions. Another standard, for example, describes the method that should be used using DSC in detail [23].

With the usage of the DSC and standardized tests, the research has evolved to the structure of the SMA and its impact on the behaviour. The effect of crystallographic material combinations significantly matters when the response of the material is measured. In the paper of Lemke and Coda [24], the direct effect of the material composition on transformation temperatures can be observed clearly. The DSC thermograph results showed that, the Cu percentage within the alloy structure significantly changes the transformation temperatures. By comparing experimental data for NiTiCu and NiTiHf, the study prescribed the affect of different material composition on characteristic of SMA.

The study of Farjam and Nematollahi [25] showed that not only the material combination, but also the manufacturing process, shape and the geometry of the specimen could interfere the characteristics of the material. Additive manufactured circular and rectangular cross sectioned specimens were tested in tensile tests and the resultant stress strain curves have come up with different results. The study concluded that the grain quality might be changed with respect to specimen size.

Although the tensile behaviour of the shape memory alloys are well defined with the standard tests [22], there is still discussion on the measurement of elastic propreties and there are no specific compressive test procedure defined for SMA mate-

rials. Therefore, studies, in order to predict the compressive behaviour of the SMA, is being done with a genuine approaches or ASTM standard for general compressive test [26] is used.

Sehitoglu et al [27] made a big step in successfully defining the compressive behaviour of SMAs. In their study, they used two specimens with different heat treatments, namely, peak-aged and over-aged. Similar to previously discussed effects, finish temper of the SMA might also effect the transformation characteristic of the material. Moreover, his study concluded that, the stress plateau observed in the tests, did not indicate the complete transformation, but a partial transformation was observed, the crystal orientation directly affected the compressive behaviour of the material and, finally the recoverable transformation strain could be raised by austenite strengthening by forming.

Miller and Lagoudas [28], studied the effects of the plastic strain on SMA transformation characteristic. The thermomechanical response of two SMAs with different element combinations, NiTi and NiTiCu were studied in detail under four different loading scenarios. These are; an elastoplastic loading of the austenite phase, a stress induced martensitic transformation, an elastic-detwinning-plastic loading of martensite and finally a thermally induced transformation under applied stress. Each case was studied repeatedly in order to observe the effect of residual plastic strain using DSC. Since $A_f$ temperature is different for both materials, the austenitic plastic loading experiment were done at 155 °C for NiTiCu and 120 °C for NiTi specimen. Both materials has shown similar response. Both materials yielded first and then linear hardening was observed. For each loading cycle, a similar characteristic was observed. NiTiCu showed lower strength under same loading while more repetition was required to reach a certain level of strain which indicates the hardening behaviour difference.

In addition to effects of heat treatment, manufacturing method, material composition and the coating are other fields of study. For material compatibility and galvanic corrosion prevention, coating on SMA studies are being a focus of interest. Hu and Wen [29] has made a study on nanocrystallites. Creating a ultra fine layer on the surface of SMA, the wearing resistance and hardness of the material has increased

while the surface friction coefficient has decreased. Similarly, Cheng and Cai [30] observed increased corrosion resistance by coating NiTi SMA with Tantalum using arc ion plating.

## 2.2 Constitutive Modelling and Numerical Implementation

Through out the years, with the understanding of the thermomechanical response of SMAs with experiments, constitutive modelling and its implementation on FEM tools have become a priority for the field. To prevent any kind of unexpected failures Tanaka [31] attempted to model the shape memory effect in 1D by using an *exponential hardening rule*. He used constant material parameters during transformation. Shortly after, Rodgers and Liang [32] proposed a new approach for 1D modelling. A *cosine hardening rule* instead of the exponential hardening model was used. Based on the $J_2$ type transformation surface, Rodgers and Liang later extended their former study to a 3D version [11], with a similar approach. The study was completed with a full analysis of a SMA bar under torsion.

Brinson [33] came up with a new model by introducing an internal variable, *Martensite Volume Fraction, MVF*. The addition of the MVF into the constitutive model proposed by Tanaka and Rodgers, improved the modelling of the response, and for the first time, material parameters were not kept constant with the introduction of MVF; the cosine hardening rule, introduced by Rodgers, was used.

Inspired by Brinson's internal variable addition, Auricchio and colleagues [34] studied on the modelling of the superelastic behaviour of SMAs. Using the MVF as the internal variable, Auricchio, compared different methods for homogenization of elastic modulus; namely, Mori-Tanaka, Voigt and Reuss. Moreover, the implementation of current 1D model into a solution algorithm was done by this study using trial and error method or *Return Mapping Algorithm (RMA)*. Auricchio used the linear hardening model in his study.

Govindjee and colleagues [35] investigated the 1D thermomechanical superelastic behaviour and shape memory effect simultaneously under loading. Their study covered plasticity in the constitutive equation with kinematic hardening plasticity. The con-

structed constitutive equation was applied to truss bar and beams. The results were accurately matching with macroscopic behaviour. Paiva and Savi [36], [37] have focused on the cyclic behaviour of SMA, the studies were built on constitutive equations constructed by Fremond [38]. Similar to Govindjee, the plastic strain was included in both studies. The internal sub-loops due to incomplete phase transformations and the tensile-compressive assymetry were modelled. These studies had an important role to correctly describe the TWSME behaviour of SMA.

Boyd and Lagoudas [39, 40] in 1996, proposed a relation between the MVF and transformation strain. Similar to a study done by Rodgers and Liang, $J_2$ type transformation surface was used. Their constitutive equation was based on Patoor [41] and Lexcellent's [42] work and generated by using Gibbs free energy function and a dissipation potential. The plastic strain was included in the constitutive equation as the irrecoverable strain. Adiabatic and isothermal transformation were compared. A polynomial hardening function was introduced.

Lagoudas and coworkers have continued their works [43] on constitutive modelling, and a unified version of thermodynamic constitutive model for SMA materials was presented. The dissipated or gained thermal energy in forward and reverse transformations were predicted by different models and a comparison was made between predicted data and experimentally measured data. For the incremental formulation of the model, the proposed unified model was applied in a finite element analysis scheme utilizing return mapping algorithm technique.

This study of Lagoudas [43] has formed a basis for the integration of the constitutive modelling of SMA to commerical finite element analysis tools such as ABAQUS. A manual [12] on how to implement SMA material modelling into ABAQUS subroutine has published shortly after the unified model was issued. This manual provides a detailed review of a user subroutine coded in FORTRAN. The unified model proposed by Lagoudas was implemented using return mapping algorithm following the study of Qidwai [44]. Although the subroutine is programmed to be used in ABAQUS, it can also be applied in any other computational program following the same method. The proposed subroutine is capable of solving 1D, 2D and 3D problems.

Apart from the studies at that time, Juhasz [45] used the transformation strain, $\epsilon^t$

which referred as *transformation induced strain (TIS)* as an internal variable. In order to represent some of the 3D effects that is not described by common macroscopic models, a new continuum model for the characterization of the general mechanical behaviour of polycrystalline SMA was presented. The main focus of the study was to model OWSME and superelasticity under various thermomechanical loading cases. The TIS tensor was generated by a new constitutive equation without plastic analogy.

Transformation induced plasticity or TRIP is studied by Lagoudas and Entchev [46, 47]. Their study proposed rate-independent thermomechanical constitutive model for dense SMAs. The hysteresis characteristic of SMAs and the effect of both transformation and plastic strains during martensitic transformation were investigated. Instead of using constant material parameters, evaluation method for material parameters was presented. They implemented their model in numerical studies using the common method return mapping algorithm. They verified their model with the experiments done on SMA strips and wires.

Based on the unification study of Lagoudas [43], Hartl and Lagoudas [3] issued another study on constitutive modelling of SMA. This study basically focused on three characteristic behaviour of SMA explicitly. Firstly, the smooth transitions which were related to martensitic transformation, during the thermal and mechanical responses are acquired. Secondly, increasing the computational accuracy by evaluating the effect of stress application on martensitic variants. Thirdly, the critical thermodynamical force approach was generalized, considering the transformation direction and stress magnitude. The study also added calibration of the model parameters which increase the correlation of two analysis result with the experiments and also the smooth hardening effect.

As the constitutive modelling of SMA has enhanced, the conventional plasticity in SMA has started to involve in the models. Wang and his colleagues [48] studied on the effects of plastic strain on the phase transformation characteristics of NiTi SMA. In order to test the stress-strain relation and energy density behaviour under plastic strain, different parts with different initial residual strain values were compared under cyclic loading. The plastic yielding which was observed only at martensite phase, was found to be affecting the stable state of stress-strain curve. Jiang and Landis [49]

have specifically worked on the modelling of plasticity on SMA. The plasticity was modeled using $J_2$-based yield surface with linear hardening. The study was specifically focused on unsymmetrical behaviour of SMA under tension and compression in combination with plasticity. The proposed model was verified by experimental observations. The plastic deformation is only observed at martensite phase. The study of Zou and Wang [50] aimed to model the SMA behaviour including plasticity. The plastic deformation was observed at martensite phase only which is compatible with the experimental results.

Scalet [51] studied on a three dimensional constitutive modelling in order to describe the plastically deformed SMA behaviour. Different than other studies, numerical implementation based on Fischer–Burmeister function was used in order to correctly predict the behaviour of the material. Similar to previously described studies, the model of Scalet was also included the plastic deformation at martensite phase only. Pseudoelastic behaviour, one way and two way shape memory affects were modeled. Petrini [52], worked particularly on NiTi alloys. The plastic behaviour was modelled by introducing new internal state variables. Also the effect of the evolution of the plastic strain, on SMA phase transformation was considered. The material model parameters calibration procedure is studied thoroughly. The resultant code was compared with the uniaxial experiments that are available in the literature.

Another study on the plasticity of SMAs, is done by Hartl [4] where both experimental and theoretical works on the formation of plastic strain and its effect on SMA material behaviour were presented. A novel 3D constitutive model was developed based on the results of SMA characterization given in literature and additional testing was done in this study. This phenomenological model describes the well-known SME, superelasticity, thermal recovery along with the evolution and effects of plastic strain. The model was also applied into finite element tools using return mapping algorithm. Plasticity was modeled with combined hardening. The generated model and finite element analysis was compared with the experimental results and consistency was achieved.

Apart from the other studies that are including plastic behaviour in SMAs, Hartl [4] has included plastic deformation at both austenite and martensite phases. Although

similar studies on plasticity in SMA exhibit no plastic deformation with transformation after elastic deformation at austenite phase, in the model of Hartl, plastic deformation at austenite phase prior to transformation took place. This thesis study refers Hartl [4] model in plasticity modelling and the existence of plastic deformation at the austenite phase is investigated.

# CHAPTER 3

# GOVERNING EQUATIONS

In this chapter, the derivation of constitutive equations of shape memory alloy and the effect of plasticity will be described in detail.

## 3.1 Continuum Mechanics

### 3.1.1 First Law of Thermodynamics: Conservation of Energy

The principle of conservation of energy basically states that rate of the total energy $E$ is equal to rate of work done $W$ on the system by external forces, the rate of heat energy $Q$ and all other types of energy rates, such as electromagnetic energy, chemical energy, surface energy. For simplicity, only $W$ and $Q$ will be included in the formulation of thermo-mechanical system.

$$\dot{E} = \dot{W} + \dot{Q}$$

Rate of the total energy, in thermo-mechanical case, can be divided into kinetic energy rate $V$ and internal energy rate $U$.

$$\dot{K} + \dot{U} = \dot{W} + \dot{Q} \tag{3.1}$$

where;

$$\dot{K} = \int_V \frac{1}{2}\rho v_i v_i dV$$
$$\dot{U} = \int_V \rho u dV$$
$$\dot{W} = \int_S t_{(n)i} v_i dS + \int_V b_i v_i dV$$
$$\dot{Q} = \int_S -q_i n_i dS + \int_V \rho r dV$$

$V$ is the volume and $S$ is the surface of a body, $r$ is the heat source, $q_i$ is the heat flux, $u$ is the specific internal energy, $t_{(n)i}$ is the traction, $b_i$ is the body force per unit mass, $v_i$ is the velocity field and $\rho$ is the density.

The rate of mechanical work done on the system $\dot{W}$ can be rewritten in terms of volume integral;

$$\dot{W} = \int_V (\sigma_{ij} v_i)_{,i} dV + \int_V b_i v_i dV$$

where $\sigma_{ij}$ is the stress tensor. Using Cauchy's equation of motion and velocity gradient decomposition, the above equation reduces to [53];

$$\dot{W} = \frac{d}{dt}\int_V \frac{1}{2}\rho v_i v_i dV + \int_V \sigma_{ij} D_{ij} dV \tag{3.2}$$

where $D_{ij}$ is the deformation rate tensor. The second term in the right hand side is known as stress power. It is defined as the mechanical work done by external forces that are not converted into kinetic energy. If the Equation 3.2 is put into Equation 3.1, the equation given below is obtained.

$$\rho \frac{du}{dt} = \sigma_{ij} D_{ij} + \rho r - q_{i,i} \tag{3.3}$$

Equation 3.3 is the general form of first law of thermodynamics and it defines that increase of the internal energy per unit volume consists of the stress power and the heat supplied by the internally distributed sources and heat flow of thermal energy through the boundary into the system.

### 3.1.2 Second Law of Thermodynamics: Principle of Entropy (Clasius-Duhem Inequality)

The second law of thermodynamics states that the internal entropy production is always greater than or equal to zero. The mathematical form of the Clasius-Duhem inequality is;

$$\frac{d}{dt}\left(\int_V \rho s dV\right) \geq \int_V \frac{\rho r}{T} dV - \int_S \frac{q_i n_i}{T} dS$$

where $s$ is specific entropy per unit mass and $T$ is temperature. The above equation can be written in terms of volume integral which will result in Clasius-Duhem inequality in local form [1];

$$\frac{ds}{dt} - \frac{r}{T} + \frac{1}{\rho T} q_{i,i} - \frac{1}{\rho T^2} \nabla T \geq 0$$

from experimental observations, it can be stated that the term $\nabla T / \rho T^2$ is always greater than zero. Therefore resultant formula of second law of thermodynamics or Clasius-Planck Inequality can be written as;

$$\frac{ds}{dt} - \frac{r}{T} + \frac{1}{\rho T} q_{i,i} \geq 0 \tag{3.4}$$

### 3.1.3 Constitutive Equations Using Laws of Thermodynamics

In order to construct a constitutive equation, firstly, dependent and independent state variables should be chosen. Any one of the thermodynamic potentials that are shown in table 3.1 can be chosen in order to get a constitutive equation. The parameter $\zeta$ shown in the table stands for a set of internal state variables to account for the loading history dependence [1].

Firstly, Equation 3.3, first law of thermodynamics, can be rewritten as;

Table 3.1: Thermodynamic Potentials and Their Relationships[1]

| Specific Thermodynamic Potentials | Relation to Internal Energy $u$ | Independent Variables |
|---|---|---|
| Internal Energy $u$ | $u$ | $s$, $\epsilon$, $\zeta$ |
| Enthalpy $h$ | $h = u - \frac{1}{\rho}\sigma_{ij}\epsilon_{ij}$ | $s$, $\sigma$, $\zeta$ |
| Helmholtz Free Energy $\psi$ | $\psi = u - sT$ | $T$, $\epsilon$, $\zeta$ |
| Gibbs Free Energy $G$ | $G = u - \frac{1}{\rho}\sigma_{ij}\epsilon_{ij} - sT$ | $T$,$\sigma$,$\zeta$ |

$$q_{i,i} = -\rho\frac{du}{dt} + \sigma_{ij}D_{ij} + \rho r \tag{3.5}$$

The term $q_{i,i}$ in Equation 3.4 can be replaced by Equation 3.3 resulting the equation;

$$\rho\dot{s}T - \rho\dot{u} + \sigma_{ij}D_{ij} \geq 0 \tag{3.6}$$

Since Gibbs free energy has been chosen as thermodynamic potential, the $\dot{u}$ term in Equation 3.6 is replaced by Gibbs free energy. Using relation between $u$ and $G$ given in Table 3.1, the Gibbs free energy rate can be written as;

$$\dot{G} = \dot{u} - \frac{1}{\rho}\dot{\sigma}_{ij}\epsilon_{ij} - \frac{1}{\rho}\sigma_{ij}\dot{\epsilon}_{ij} - \dot{s}T - s\dot{T} \tag{3.7}$$

replacing the $\dot{u}$ in Equation 3.6, using Equation 3.7, and assuming $D_{ij} = \dot{\epsilon}_{ij}$ the equation becomes;

$$-\rho\dot{G} - \rho s\dot{T} - \dot{\sigma}_{ij}\dot{\epsilon}_{ij} \geq 0 \tag{3.8}$$

Since $G$ is a function of $\sigma$, $T$ and $\boldsymbol{\nabla}T = g$ [1] it can be written as;

$$\dot{G} = \frac{\partial G}{\partial \boldsymbol{\sigma}} : \dot{\boldsymbol{\sigma}} + \frac{\partial G}{\partial T}\dot{T} + \frac{\partial G}{\partial g}\dot{g} \tag{3.9}$$

where : is used for double dot product (e.g. $\sigma_{ij}\epsilon_{ij} = \boldsymbol{\sigma} : \boldsymbol{\epsilon}$) and bold characters are used for tensors (e.g. $\sigma_{ij} = \boldsymbol{\sigma}$). Therefore, if Equation 3.7 is put into Equation 3.8;

$$-\rho\left(\frac{\partial G}{\partial \boldsymbol{\sigma}} : \dot{\boldsymbol{\sigma}} + \frac{\partial G}{\partial T}\dot{T} + \frac{\partial G}{\partial g}\dot{g}\right) - \rho s\dot{T} - \dot{\boldsymbol{\sigma}} : \boldsymbol{\epsilon} \geq 0 \tag{3.10}$$

and using the quadratic polynomial form of the Gibbs free energy and considering $\partial G/\partial g = 0$,

$$\begin{aligned} G = &-\frac{1}{2\rho}\boldsymbol{\sigma} : \mathbf{S} : \boldsymbol{\sigma} - \frac{1}{\rho}\boldsymbol{\sigma} : \boldsymbol{\alpha}(T - T_0) \\ &+c[(T - T_0) - T\ln(\frac{T}{T_0})] - s_0 T + u_0 \end{aligned} \tag{3.11}$$

we obtain

$$s = -\frac{\partial G}{\partial T} = \frac{1}{\rho}\boldsymbol{\sigma} : \boldsymbol{\alpha} + c\ln(\frac{T}{T_0}) + s_0 \tag{3.12}$$

$$\boldsymbol{\epsilon} = -\rho\frac{\partial G}{\partial \boldsymbol{\sigma}} = \mathbf{S} : \boldsymbol{\sigma} + \boldsymbol{\alpha}(T - T_0) \tag{3.13}$$

## 3.2 Constitutive Modelling of Shape Memory Alloys

### 3.2.1 Internal State Variables and Assumptions of Shape Memory Alloys

The first step in construction of constitutive equation is choosing the correct internal state variables. Considering the important role that they have, it would be convenient to choose transformation strain $\boldsymbol{\epsilon}^t$ and martensitic volume fraction $\xi$ as the internal state variables of constitutive equation. Martensitic volume fraction $\xi$ is defined as the ratio of martensite volume to the whole volume. Therefore its value can be between $0$ and $1$.

Previous chapter states that the Gibbs free energy, as a thermodynamic potential, is a function of independent state variables $\boldsymbol{\sigma}$ and $T$. However with the introduction of

new internal state variables, the Gibbs free energy can be rewritten as a function of $\xi$ and $\boldsymbol{\epsilon}^t$ as well. For shape memory alloys, the explicit form of Gibbs free energy is [1];

$$\begin{aligned} G = -\frac{1}{2\rho}\boldsymbol{\sigma} : \boldsymbol{S}(\xi) : \boldsymbol{\sigma} - \frac{1}{\rho}\boldsymbol{\sigma} : [\boldsymbol{\alpha}(\xi)(T - T_0) + \boldsymbol{\epsilon}^t] \\ +c(\xi)[(T - T_0) - T\ln(\frac{T}{T_0})] - s_0(\xi)T + u_0(\xi) + \frac{1}{\rho}f^t(\xi) \end{aligned} \tag{3.14}$$

where $T_0$ is reference temperature and $\mathbf{S}$, $\boldsymbol{\alpha}$, $c$, $s_0$, $u_0$, $f^t$ are the fourth-order effective compliance tensor, the second-order effective thermal expansion tensor, the effective specific heat, the effective specific entropy at the reference state, the effective specific internal energy at the reference state and the hardening function, respectively. The effective term is directly comes from the current state of the material and these parameters can be calculated with;

$$\begin{aligned} \mathbf{S}(\xi) &= \mathbf{S}^A - \xi(\mathbf{S}^M - \mathbf{S}^A) = \mathbf{S}^A - \xi\Delta\mathbf{S} \\ \boldsymbol{\alpha}(\xi) &= \boldsymbol{\alpha}^A - \xi(\boldsymbol{\alpha}^M - \boldsymbol{\alpha}^A) = \boldsymbol{\alpha}^A - \xi\Delta\boldsymbol{\alpha} \\ c(\xi) &= c^A - \xi(c^M - c^A) = c^A - \xi\Delta c \\ s_0(\xi) &= s_0^A - \xi(s_0^M - s_0^A) = s_0^A - \xi\Delta s_0 \\ u_0(\xi) &= u_0^A - \xi(u_0^M - u_0^A) = u_0^A - \xi\Delta u_0 \end{aligned}$$

which gives;

$$\boldsymbol{\epsilon} = \boldsymbol{S}(\xi) : \boldsymbol{\sigma} + \boldsymbol{\alpha}(\xi)(T - T_0) + \boldsymbol{\epsilon}^t \tag{3.15}$$

and

$$s = \frac{1}{\rho}\boldsymbol{\sigma} : \boldsymbol{\alpha}(\xi) + c(\xi)\ln(\frac{T}{T_0}) + s_0(\xi)$$

The local form of entropy inequality for shape memory alloys can be obtained as;

$$-\rho\left(\frac{\partial G}{\partial \boldsymbol{\epsilon}^t} : \dot{\boldsymbol{\epsilon}}^t + \frac{\partial G}{\partial \xi}\dot{\xi}\right) \geq 0 \tag{3.16}$$

And using Equation 3.9 and 3.13, Equation 3.16 also can be reduced to;

$$\boldsymbol{\sigma} : \dot{\boldsymbol{\epsilon}}^t + \left( -\rho \frac{\partial G}{\partial \xi} \dot{\xi} \right) \geq 0 \tag{3.17}$$

### 3.2.2 Flow Rule of Transformation Strain

Since the total strain, entropy and local form of entropy inequality are obtained, the evolution of internal state variables, $\xi$ and $\epsilon^t$, should be carried out. At this point one major assumption should be made. Any change in microstructural state of material directly results in martensitic volume fraction, $\xi$, change [1]. Therefore, below formulation can be constructed as flow rule.

$$\dot{\boldsymbol{\epsilon}}^t = \boldsymbol{\Lambda^t} \dot{\xi} \tag{3.18}$$

where $\boldsymbol{\Lambda^t}$ is the transformation tensor. Transformation tensor is used to determine the direction of the transformation and it has different values for forward and reverse transformation as shown below:

$$\boldsymbol{\Lambda^t} = \begin{cases} \frac{3}{2} H \frac{\boldsymbol{\sigma'}}{\bar{\sigma}'}, & \text{if} \qquad \dot{\xi} > 0, \\ \frac{\boldsymbol{\epsilon}^{t-r}}{\xi^{t-r}}, & \text{if} \qquad \dot{\xi} < 0. \end{cases} \tag{3.19}$$

$\boldsymbol{\sigma'}$, $\bar{\sigma}'$, $\boldsymbol{\epsilon}^{t-r}$, $\xi^{t-r}$ and $H$ in 3.19 are deviatoric stress tensor, effective von Misses stress, transformation strain at the reversal point, MVF at reversal point and a variable associated with maximum transformation strain magnitude respectively. They can be calculated using below formulas;

$$\begin{aligned} \boldsymbol{\sigma'} &= \boldsymbol{\sigma} - \frac{1}{3} tr(\boldsymbol{\sigma}) \\ \bar{\sigma}' &= \sqrt{\frac{3}{2} \boldsymbol{\sigma'} : \boldsymbol{\sigma'}} \\ H(\sigma) &= H_{max}(1 - e^{k\bar{\sigma}'}) \end{aligned} \tag{3.20}$$

where $H_{max}$ and $k$ are material parameters that can be found experimentally [3].

If the flow rule 3.18 is inserted into Clasius-Planck inequality 3.17, the thermodynamic force, $\pi^t$ can be obtained.

$$\left(\boldsymbol{\sigma} : \boldsymbol{\Lambda^t} - \rho\frac{\partial G}{\partial \xi}\right)\dot{\xi} = \pi^t\dot{\xi} \geq 0 \tag{3.21}$$

where $\pi$ is;

$$\begin{aligned}\pi^t = \boldsymbol{\sigma} : \boldsymbol{\Lambda^t} + \frac{1}{2}\boldsymbol{\sigma} : \Delta\boldsymbol{S} : \boldsymbol{\sigma} + \boldsymbol{\sigma} : [\Delta\boldsymbol{\alpha}(T - T_0)] \\ -\rho\Delta c[(T - T_0) - T\ln(\frac{T}{T_0})] + \rho\Delta s_0 T - \rho\Delta u_0 - \frac{\partial f^t}{\partial \xi}\end{aligned} \tag{3.22}$$

The thermodynamic force is used to decide whether the transformation is occurring and if it is, in which direction. When $\pi^t$ reaches a critical threshold value $Y^t$ or $-Y^t$, it is assumed that the transformation will occur. When $\dot{\xi}$ is positive, meaning that material is undergoing forward transformation (from austenite to martensite), $\pi^t$ needs to be a positive threshold value ($Y^t$) in order to satisfy Clasius-Planck inequality 3.21. When $\dot{\xi}$ is negative, meaning that material is undergoing reverse transformation (from martensite to austenite), $\pi^t$ needs to be a negative threshold value ($-Y^t$) in order to satisfy Clasius-Planck inequality 3.21.

If there are no transformation which means $\dot{\xi}$ is zero, Clasius-Planck inequality 3.21 is satisfied without considering the value of $\pi^t$.

The assumptions above, allows us to capture the transformation occurence in both forward and reverse directions with the introduction of a transformation function, $\Phi^t$.

$$\Phi^t = \begin{cases}\pi^t - Y^t, & \text{if} \qquad \dot{\xi} > 0 \\ -\pi^t - Y^t, & \text{if} \qquad \dot{\xi} < 0\end{cases}$$

whenever $\Phi^t$ is zero, it indicates that transformation is occurring. Considering the equation above, Kuhn-Tucker conditions can be constructed as;

$$\dot{\xi} \geq 0 \qquad \Phi^t = \pi^t - Y^t \leq 0 \qquad \Phi^t\dot{\xi} = 0$$

$$\dot{\xi} \leq 0 \qquad \Phi^t = -\pi^t - Y^t \leq 0 \qquad \Phi^t \dot{\xi} = 0$$

Kuhn-Tucker conditions should always be satisfied during both transformation occurence and thermoelastic response of the material.

### 3.2.3 Hardening Function

The hardening function selection is another important point while constructing a constitutive equation. As can be seen from the Equation 3.14, the hardening function, $f^t$ directly affects the energy formulation. There are different way to approach hardening function definition and most of them are based on experimental data. In this thesis, the proposed model by Lagoudas [43] will be used. In this approach, considering the reversibility of transformation, the forward and reverse transformation hardening energy summation is assumed to be zero. Moreover, the smooth transition from elastic deformation to transformation is also included. The hardening functions for both forward and reverse transformation can be written as;

$$f^t(\xi)_{fwd} = \frac{1}{2} a_1 (1 + \xi^{n_1} - (1-\xi)^{n_2})) + a_3$$

and

$$f^t(\xi)_{rev} = \frac{1}{2} a_2 (1 + \xi^{n_3} - (1-\xi)^{n_4})) - a_3$$

where $n_1$, $n_2$, $n_3$, $n_4$ are the coefficients that can be determined from experimental studies and can only take the values higher then 0 and lower or equal to 1 and $a_1$, $a_2$, $a_3$ are model parameters. While defining the constitutive model, model parameters are needed to be defined as well. Model parameters are important to decide whether the model is theoretically and practically correct and can be used in engineering applications. Similar to, hardening function, model parameters can also be changed according to approaches used. Model parameters must be calibrated with a stress level that the response of the material is experimentally measured and already known [3]. The model parameters and their formulation in terms of material parameters are given below.

$$a_1 = \rho \Delta s_0 (M_f - M_s)$$

$$a_2 = \rho\Delta s_0(A_s - A_f)$$

$$a_3 = \frac{-a_1}{4}\left(1 + \frac{1}{n_1+1} - \frac{1}{n_2+1}\right) + \frac{a_2}{4}\left(1 + \frac{1}{n_3+1} - \frac{1}{n_4+1}\right)$$

$$\rho\Delta u_0 = \frac{\rho\Delta s_0}{2}(M_s + A_f)$$

$$Y_0^t = \frac{\rho\Delta s_0}{2}(M_s - A_f) - a_3$$

### 3.3 Constitutive Modelling of Shape Memory Alloys Including Plasticity

With the introduction of the plasticity, the total energy formulation changes respectively. The affects of the plastic strain, $\epsilon^p$ and the plastic hardening $f^p$ are included in order to simulate the energy dissipation via plastic deformation. The Equation 3.14 includes only transformation strain effect along with thermal, entropy and internal energy. Since austenite and martensite phases have different plasticity characteristics, each phase should be evaluated separately. Therefore, the open form of Equation 3.14 should be taken into consideration. For simplicity, the open form is divided into three sections namely, austenite $G^A$, martensite $G^M$ and energy of mixing $G^{mix}$. The open form of energy formulation including plasticity can be written as [4];

$$\begin{aligned} G(\boldsymbol{\sigma}, T, \boldsymbol{\epsilon}^t, f^t, \boldsymbol{\epsilon}^p, f_A^p, f_M^p, \boldsymbol{\beta}) = (1-\xi)G^A(\boldsymbol{\sigma}, T, \boldsymbol{\epsilon}^p, f_A^p, \boldsymbol{\beta}) \\ +\xi G^M(\boldsymbol{\sigma}, T, \boldsymbol{\epsilon}^p, f_M^p, \boldsymbol{\beta}) + G^{mix}(\boldsymbol{\sigma}, \boldsymbol{\epsilon}^t, f^t) \end{aligned} \tag{3.23}$$

where

$$\begin{aligned} G^\gamma(\boldsymbol{\sigma}, T, \boldsymbol{\epsilon}^p, f_\gamma^p, \boldsymbol{\beta}) = -\frac{1}{2\rho}\boldsymbol{\sigma} : \boldsymbol{S}^\gamma : \boldsymbol{\sigma} - \frac{1}{\rho}(\boldsymbol{\sigma} - \boldsymbol{\beta}) : \boldsymbol{\epsilon}^p + \frac{1}{\rho}f_\gamma^p \\ -\frac{1}{2\rho K_\beta^\gamma}\boldsymbol{\beta} : \boldsymbol{\beta} - \frac{1}{\rho}\boldsymbol{\sigma} : \boldsymbol{\alpha}(T - T_0) + c[(T - T_0) - T\ln(\frac{T}{T_0})] - s_0^\gamma T + u_0^\gamma \end{aligned} \tag{3.24}$$

$\gamma$ can be either $A$ or $M$ which stand for austenite and martensite, $\boldsymbol{\beta}$ is the backstress, $K_\beta$ is the kinematic hardening modulus, $f^t$ is the hardening function for transformation, $f^p$ is the hardening function for plasticity and $\boldsymbol{\epsilon}^p$ is plastic strain. The energy of mixing can be written as;

$$G^{mix}(\boldsymbol{\sigma}, \boldsymbol{\epsilon}^t, f^t) = -\frac{1}{\rho}\boldsymbol{\sigma} : \boldsymbol{\epsilon}^t + \frac{1}{\rho}f^t \tag{3.25}$$

using Equation 3.23 and Equation 3.15 the total strain including plasticity can be calculated as;

$$\boldsymbol{\epsilon} = \boldsymbol{S}(\xi) : \boldsymbol{\sigma} + \boldsymbol{\alpha}(\xi)(T - T_0) + \boldsymbol{\epsilon^t} + \boldsymbol{\epsilon^p} \tag{3.26}$$

The flow rule for transformation strain which is defined in the previous section does not affected from plasticity addition and remains the same. However with the introduction of backstress $\boldsymbol{\beta}$, the formulation of stress at Equation 3.19 is changed as;

$$\boldsymbol{\sigma}_t^{eff} = \boldsymbol{\sigma} + \boldsymbol{\beta}$$

In order to observe the affect of backstress, $\boldsymbol{\sigma}_t^{eff}$ should be used in Equations 3.20 instead of $\boldsymbol{\sigma}$.

Similar to new definition of transformation stress, the plastic strain flow rule should be constructed. Considering the Prandtl-Reuss theory of plasticity [53], the rate of the plastic strain should be coaxial with deviatoric stress. Using von Mises yield criterion, the rate of the plastic strain can be formulated as;

$$\dot{\boldsymbol{\epsilon}}^p = \boldsymbol{\Lambda}^p \dot{\overline{\epsilon}}^p \tag{3.27}$$

where $\overline{\epsilon}^p$ is the effective rate of plastic strain and it can be calculated via;

$$\dot{\overline{\epsilon}}^p = \sqrt{(\frac{2}{3}\dot{\boldsymbol{\epsilon}}^p \dot{\boldsymbol{\epsilon}}^p)}$$

and

$$\boldsymbol{\Lambda}^p = \frac{3}{2}\frac{\boldsymbol{\sigma}_p^{eff'}}{\bar{\sigma}_p^{eff}}$$

where;

$$\begin{aligned}
\boldsymbol{\sigma}_p^{eff} &= \boldsymbol{\sigma} - \boldsymbol{\beta} \\
\boldsymbol{\sigma}_p^{eff'} &= \boldsymbol{\sigma}_p^{eff} - \frac{1}{3} tr(\boldsymbol{\sigma}_p^{eff}) \\
\bar{\sigma}_p^{eff'} &= \sqrt{\frac{3}{2}\boldsymbol{\sigma}_p^{eff'}}
\end{aligned} \tag{3.28}$$

Equation 3.20 and Equation 3.28 are basically the same formulation except the sigma definition incorporates by backstress.

In equation 3.24, the hardening function $f_\gamma^p$ is introduced. In order the include the affect of hardening evolution function, the rate of the hardening energy should be defined, in similar manner with the flow rule. The hardening energy rate of the plasticity can be calculated by [4];

$$\dot{f}_\gamma^p = [(Y_m^\gamma - Y_0^\gamma)(1 - e^{-C_H \bar{\epsilon}^p}) - K_\beta^\gamma \bar{\epsilon}^p]\dot{\bar{\epsilon}}^p = \tilde{f}_\gamma^p \dot{\bar{\epsilon}}^p$$

where $\gamma$ can be either $A$ or $M$.

In the plasticity models with kinematic hardening, the backstress $\boldsymbol{\beta}$ is always proportional to the rate of $\boldsymbol{\epsilon}^p$ and the kinematic hardening modulus $K_\beta$ is a constant. Since shape memory alloys introduce a phase change, the backstress is assumed to be a function of Martensitic Volume Fraction, $\xi$, as well. The formulation of $\boldsymbol{\beta}$ can be written as;

$$\boldsymbol{\beta} = ((\xi)K_\beta^M + (1-\xi)K_\beta^A)\boldsymbol{\epsilon}^p + \boldsymbol{\beta}_0$$

where $K_\beta^M$ and $K_\beta^A$ are kinematic hardening modulus of martensite and austenite respectively and $\boldsymbol{\beta_0}$ is the initial backstress.

Another important assumption made in order to correctly model the plasticity of SMA, is the definition of critical effective plastic strain. As the study by Hartl [4] suggests, plastic deformation affects the transformation process and creates an irrecoverable martensitic volume fraction, $\xi_{irr}$. Up to an critical value, $\xi_{irr}$ is increases

proportionally, once the critical point is reached or exceeded, $\xi_{irr}$ becomes one, meaning that part will no longer be able transform back to austenite. The conditional calculation of the $\xi_{irr}$ is given in Equation 3.29.

$$\xi_{irr} = \begin{cases} \frac{\bar{\epsilon}^p}{\bar{\epsilon}^p_{crit}}, & \text{if} \qquad \bar{\epsilon}^p < \bar{\epsilon}^p_{crit} \\ 1, & \text{if} \qquad \bar{\epsilon}^p \geq \bar{\epsilon}^p_{crit} \end{cases} \tag{3.29}$$

The value of the critical effective plastic strain is found empirically changes for different material combitinations. Similar to, equation 3.21, the plasticity effect should also be taken into account to satisfy Clasius-Duhem Inequality.

$$\left((\boldsymbol{\sigma} - \boldsymbol{\beta}) : \boldsymbol{\Lambda}^p - ((1-\xi)\tilde{f}^p_A + \xi \tilde{f}^p_M)\right) \dot{\bar{\epsilon}}^p = \pi^p \dot{\bar{\epsilon}}^p \geq 0 \tag{3.30}$$

The plasticity processes are assumed to begin once the thermodynamic force $\pi^p$ reaches to a threshold value of $Y^p$. At this point, similar to transformation function, plastic yield function, $\Phi^p$ can be defined. Both transformation function and plastic yield function should be checked at the same time in order to correctly model the behaviour of the material. Considering the values of the transformation function and plastic yield function; the material can undergo each one of these separately or simultaneously.

$$\Phi^p = \pi^p - Y^p \leq 0$$

and an additional Kuhn-Tucker condition for plasticity can be constructed as;

$$\dot{\bar{\epsilon}}^p \geq 0 \qquad \Phi^p = \pi^p - Y^p \leq 0 \qquad \Phi^p \dot{\bar{\epsilon}}^p = 0$$

These equations suggest that, the transformation may only occur if $\Phi^p$ is equal to zero. Otherwise, no plastic deformation is taken place. With the introduction of the flow rule, hardening function evolution equation and thermodynamic force, the constitutive equation is constructed including plasticity effect. Therefore, further study about stress and strain relation can be made using iterative approach.

## 3.4 Numerical Implementation of the Model

Although the introduced constitutive model is able to foresee the behaviour of the SMA, the complex geometries and conditions still require an implementation into a finite element tool. In order to solve such problems, a user material subroutine (UMAT) is used in ABAQUS finite framework [54]. The basic structure of the proposed subroutine code can be divided into two parts. In the first part, the code focuses on the internal state variables. Four internal state variables are found using four equations by Newton-Rhapson method. In each iteration, the internal state variables are updated until, Kuhn-Tucker conditions satisfied and residuals calculated via flow rules are minimized. The second part, mainly focuses on, to give a stiffness matrix and stress increment with respect to temperature to ABAQUS global solver. The code of the subroutine, covers the implementation of the presented constitutive model and the stress increments. Once ABAQUS obtains these data, it can find the local stress and strain values.

### 3.4.1 Internal State Variable Calculation

As the method used by Karakalas [2] describes, for the SMA constitutive equations without plasticity, the stress calculated by the global solver is calculated by total strain which is a function of displacement and internal state variables such as $\boldsymbol{\epsilon}^t$ and $\xi$. While UMAT is in the thermoelastic prediction step (the initial step), the internal variables are assumed to be the initially given data or values that obtained in the last successfully converged increment. Using these values, the current stress vector and related derivatives are calculated. The current stress vector is used to calculate both of the forward and reverse transformation function, $\Phi^t$, values. The calculated transformation values are substracted from the last increment and the obtained difference and the current value of $\Phi^t$ are used to determine the occurrence of the transformation and the direction of it. If the difference and current value are greater than or equal to zero, the Kuhn-Tucker conditions are violated and transformation is occurring, if the difference is smaller, the response is purely elastic without any transformation. In case of a transformation, the values of $\boldsymbol{\epsilon}^t$ and $\xi$ should be updated using Newton-Rhapson method so that the Kuhn-Tucker conditions are satisfied again. The Newton-Rhapson

equation used in the code and the update process using obtained delta values are given below.

The whole procedure is described in Figure 3.1. In order to satisfy the Kuhn-Tucker condition, transformation function $\Phi^t$ should be zero during the transformation. Similarly, transformation strain residual $\boldsymbol{R}_t$ which is calculated using flow rule, should also be zero during the transformation. Strain residual is calculated as given below.

$$\begin{bmatrix} \frac{\partial \boldsymbol{R}_t^{t+\Delta t}}{\partial \boldsymbol{\epsilon}_t^{t+\Delta t}} & \frac{\partial \boldsymbol{R}_t^{t+\Delta t}}{\partial \xi^{t+\Delta t}} \\ \frac{\partial \Phi^{t+\Delta t}}{\partial \boldsymbol{\epsilon}_t^{t+\Delta t}} & \frac{\partial \Phi^{t+\Delta t}}{\partial \xi^{t+\Delta t}} \end{bmatrix}^{-1} \begin{bmatrix} \boldsymbol{R}_t^{t+\Delta t} \\ \Phi^{t+\Delta t} \end{bmatrix} = \begin{bmatrix} \Delta \boldsymbol{\epsilon}^t \\ \Delta \xi \end{bmatrix} \tag{3.31}$$

and

$$\begin{bmatrix} \boldsymbol{\epsilon}^t \\ \xi \end{bmatrix} + \begin{bmatrix} \Delta \boldsymbol{\epsilon}^t \\ \Delta \xi \end{bmatrix} = \begin{bmatrix} \boldsymbol{\epsilon}^t \\ \xi \end{bmatrix} \tag{3.32}$$

$$\boldsymbol{R}_t = (-\boldsymbol{\epsilon}^t_{current} + \boldsymbol{\epsilon}^t_{previous}) + \boldsymbol{\Lambda}^t(-\xi_{current} + \xi_{previous}) \tag{3.33}$$

These two equations are used to find $\boldsymbol{\epsilon}^t$ and $\xi$. At each increment, the deltas of internal state variables are calculated using equation 3.32 and the corresponding $\Phi^t$ and $\boldsymbol{R}_t$ values are tried to be converged to zero. If these two values are within the pre-defined tolerances, the iteration is over. Otherwise, a correction procedure is applied and new values of $\boldsymbol{\epsilon}^t$ and $\xi$ are calculated based on the previous increment with equations 3.31 and 3.32 again. Figure 3.2 shows the diagram for the $\boldsymbol{\epsilon}^t$ and $\xi$ calculation procedure.

Based on the study of Hartl [4], plasticity effect on the SMA have added in the code by following a similar manner to transformation effect. In addition to $\boldsymbol{\epsilon}^t$ and $\xi$, $\boldsymbol{\epsilon}^p$ and $\bar{\epsilon}^p$ are considered as internal variables as well. The stress vector and the related derivatives at the current increment is used to calculate plastic yield function, $\Phi^p$, value. If the calculated plastic yield function is greater than or equal to zero, the Kuhn-Tucker conditions are violated meaning that plastic deformation is occurring, if plastic yield function is lower than zero, the response is purely elastic. If plastic deformation is detected, the values of $\boldsymbol{\epsilon}^p$ and $\bar{\epsilon}^p$ should be updated using the same Newton-Rhapson method used in transformation case. The iterations are done up to a point where Kuhn-Tucker conditions are satisfied and plastic strain residual $\boldsymbol{R}_p$ is

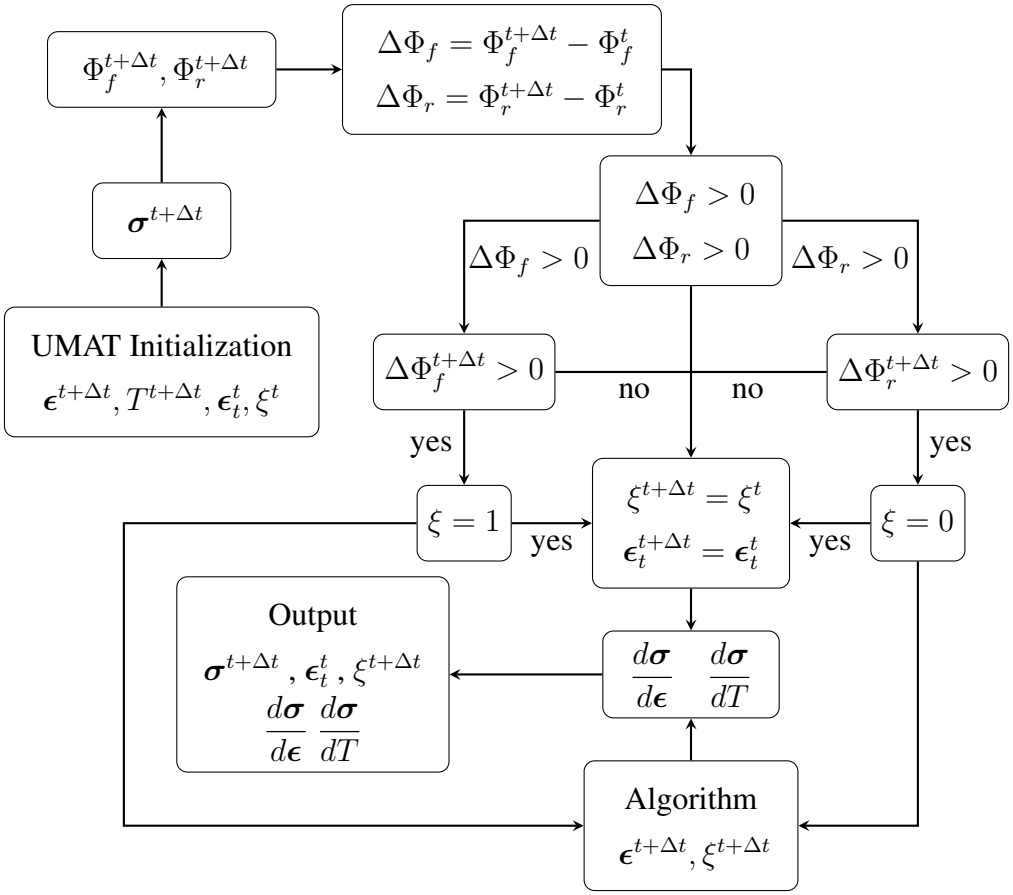


Figure 3.1: The Diagram of the Subroutine Including Transformation [2]

zero. Plastic strain residual is calculated as;

$$\boldsymbol{R}_p = (-\boldsymbol{\epsilon}^p_{current} + \boldsymbol{\epsilon}^p_{current}) + \boldsymbol{\Lambda}^p(-\bar{\epsilon}^p_{current} + \bar{\epsilon}^p_{previous}) \tag{3.34}$$

While the new $\boldsymbol{\epsilon}^p$ and $\bar{\epsilon}^p$ are being calculated iteratively, the Newton-Rhapson method uses both of the plastic yield function and plastic strain residual. Therefore in each iteration, two unknown is calculated via two separate equation as can be seen below.

$$\begin{bmatrix} \frac{\partial \boldsymbol{R}_p^{t+\Delta t}}{\partial \boldsymbol{\epsilon}_p^{t+\Delta t}} & \frac{\partial \boldsymbol{R}_p^{t+\Delta t}}{\partial \bar{\epsilon}_p^{t+\Delta t}} \\ \frac{\partial \Phi_p^{t+\Delta t}}{\partial \boldsymbol{\epsilon}_p^{t+\Delta t}} & \frac{\partial \Phi_p^{t+\Delta t}}{\partial \bar{\epsilon}_p^{t+\Delta t}} \end{bmatrix}^{-1} \begin{bmatrix} \boldsymbol{R}_p^{t+\Delta t} \\ \Phi_p^{t+\Delta t} \end{bmatrix} = \begin{bmatrix} \Delta\boldsymbol{\epsilon}^p \\ \Delta\bar{\epsilon}^p \end{bmatrix} \tag{3.35}$$

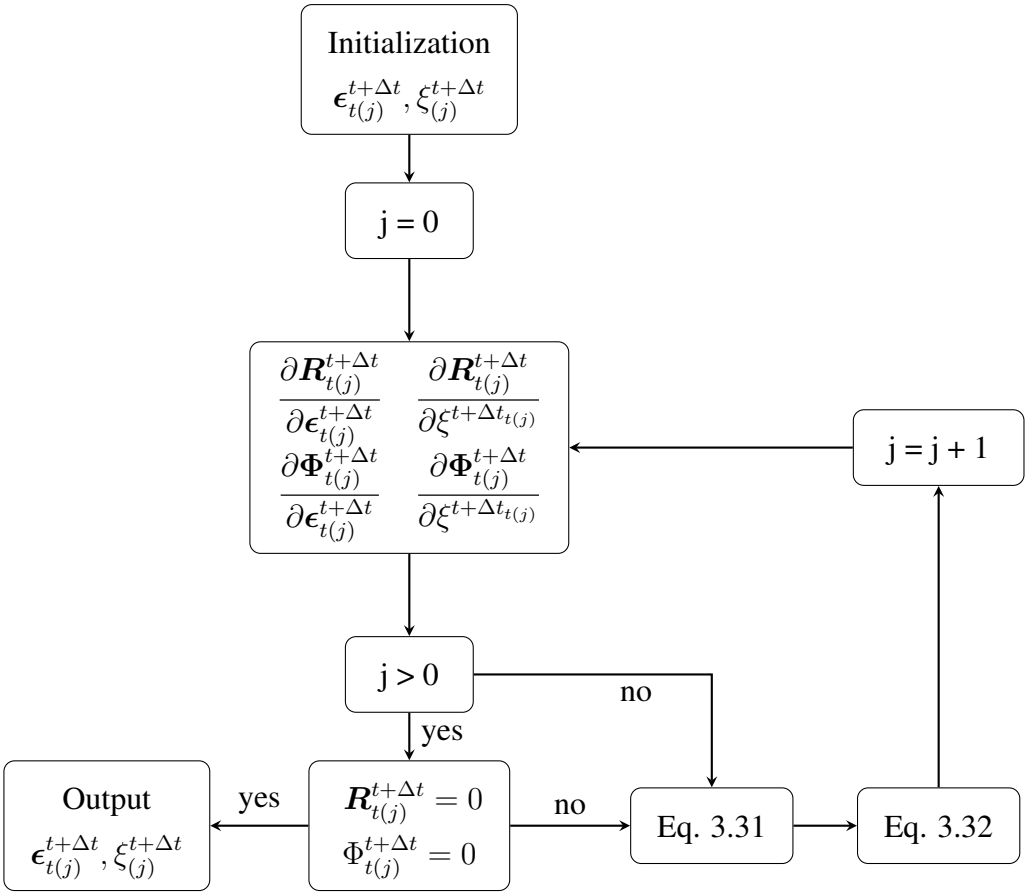


Figure 3.2: The Procedure of $\boldsymbol{\epsilon}^t$ and $\xi$ Calculation via Return Mapping Algorithm [2]

and

$$\begin{bmatrix} \boldsymbol{\epsilon}^p \\ \bar{\epsilon}^p \end{bmatrix} + \begin{bmatrix} \Delta\boldsymbol{\epsilon}^p \\ \Delta\bar{\epsilon}^p \end{bmatrix} = \begin{bmatrix} \boldsymbol{\epsilon}^p \\ \bar{\epsilon}^p \end{bmatrix} \tag{3.36}$$

Similar to pure transformation case, if $\Phi^p$ and $\boldsymbol{R}_p$ that are calculated with new values of $\boldsymbol{\epsilon}^p$ and $\bar{\epsilon}^p$, are within the pre-defined tolerances, the iteration is over. Otherwise, a correction procedure is applied. The code is modified such that in each increment both of the transformation function and plastic yield function is checked simultaneously following the same Newton-Rhapson method.

### 3.4.2 Constitutive Relation Implementation

Once the satisfactory values of $\xi$, $\boldsymbol{\epsilon}^t$, $\bar{\epsilon}^p$ and $\boldsymbol{\epsilon}^p$ are obtained by Newton-Rhapson method for the current state, the stifness matrix and the stress increment with respect to temperature can be given as an input to ABAQUS global solver. Considering the strain definition in Equation 3.26, the differential form can be written as;

$$d\boldsymbol{\epsilon} = \frac{\partial \boldsymbol{\epsilon}}{\partial \boldsymbol{\sigma}} d\boldsymbol{\sigma} + \frac{\partial \boldsymbol{\epsilon}}{\partial \xi} d\xi + \frac{\partial \boldsymbol{\epsilon}}{\partial T} dT + \frac{\partial \boldsymbol{\epsilon}}{\partial \boldsymbol{\epsilon}^t} d\boldsymbol{\epsilon}^t + \frac{\partial \boldsymbol{\epsilon}}{\partial \boldsymbol{\epsilon}^p} d\boldsymbol{\epsilon}^p \tag{3.37}$$

where

$$\begin{aligned}
\frac{\partial \boldsymbol{\epsilon}}{\partial \boldsymbol{\sigma}} &= \boldsymbol{S} \\
\frac{\partial \boldsymbol{\epsilon}}{\partial \xi} &= \Delta \boldsymbol{S}\boldsymbol{\sigma} + \Delta \boldsymbol{\alpha}(\Delta T) \\
\frac{\partial \boldsymbol{\epsilon}}{\partial T} &= \boldsymbol{\alpha} \\
\frac{\partial \boldsymbol{\epsilon}}{\boldsymbol{\epsilon}^t} &= I \\
\frac{\partial \boldsymbol{\epsilon}}{\boldsymbol{\epsilon}^p} &= I
\end{aligned}$$

$I$ stands for identity matrix. The terms $d\boldsymbol{\epsilon}^t$ and $d\boldsymbol{\epsilon}^p$ can be rewritten using flow rule Equations 3.18 and 3.27 respectively.

$$d\boldsymbol{\epsilon}^t = d\xi \boldsymbol{\Lambda}^t + \Delta\xi \frac{\partial \boldsymbol{\Lambda}^t}{\boldsymbol{\sigma}} \tag{3.38}$$

$$d\boldsymbol{\epsilon}^p = d\bar{\epsilon}^p \boldsymbol{\Lambda}^p + \Delta\bar{\epsilon}^p \frac{\partial \boldsymbol{\Lambda}^p}{\boldsymbol{\sigma}} \tag{3.39}$$

Replacing the terms in Equation 3.37 with Equations 3.38 and 3.39;

$$\begin{aligned}
d\boldsymbol{\epsilon} = (\boldsymbol{S} + \Delta\xi \frac{\partial \boldsymbol{\Lambda}^t}{\partial \boldsymbol{\sigma}} + \Delta\bar{\epsilon}^p \frac{\partial \boldsymbol{\Lambda}^p}{\partial \boldsymbol{\sigma}}) d\boldsymbol{\sigma} \\
+(\Delta \boldsymbol{S}\boldsymbol{\sigma} + \Delta\boldsymbol{\alpha}\Delta T + \boldsymbol{\Lambda^t}) d\xi + (\boldsymbol{\Lambda}^p) d\bar{\epsilon}^p + (\boldsymbol{\alpha}) dT
\end{aligned} \tag{3.40}$$

can be obtained. For transformation and yield function ($\Phi^t$, $\Phi^p$), consistency condition suggests, they both should be zero. Therefore it can be stated that;

$$d\Phi^t = \frac{\partial \Phi^t}{\partial \boldsymbol{\sigma}} d\boldsymbol{\sigma} + \frac{\partial \Phi^t}{\partial T} dT + \frac{\partial \Phi^t}{\partial \xi} d\xi = 0$$

and

$$d\Phi^p = \frac{\partial \Phi^p}{\partial \boldsymbol{\sigma}} d\boldsymbol{\sigma} + \frac{\partial \Phi^p}{\partial \xi} d\xi + \frac{\partial \Phi^p}{\partial \bar{\epsilon}^p} d\bar{\epsilon}^p = 0$$

should be achieved, during transformation and yielding. Therefore $d\xi$ and $d\bar{\epsilon}^p$ can be rewritten as;

$$d\xi = -\frac{\overline{\frac{\partial \Phi^t}{\partial \boldsymbol{\sigma}}}}{\overline{\frac{\partial \Phi^t}{\partial \xi}}} d\boldsymbol{\sigma} - \frac{\overline{\frac{\partial \Phi^t}{\partial T}}}{\overline{\frac{\partial \Phi^t}{\partial \xi}}} dT \tag{3.41}$$

$$d\bar{\epsilon}^p = -\frac{\overline{\frac{\partial \Phi^p}{\partial \boldsymbol{\sigma}}}}{\overline{\frac{\partial \Phi^p}{\partial \bar{\epsilon}^p}}} d\boldsymbol{\sigma} - \frac{\overline{\frac{\partial \Phi^p}{\partial \xi}}}{\overline{\frac{\partial \Phi^p}{\partial \bar{\epsilon}^p}}} d\xi \tag{3.42}$$

If $d\xi$ and $d\bar{\epsilon}^p$ are replaced with 3.41 and 3.42, in equation 3.40, the relation between stress, strain and temperature can be obtained.

$$d\boldsymbol{\epsilon} = (OC_1 - OC_2 A_1 - OC_3 A_2) d\boldsymbol{\sigma} + (\boldsymbol{\alpha} - OC_2 A_3 + OC_3 A_4) dT \tag{3.43}$$

where

$$OC_1 = \boldsymbol{S} + \Delta\xi \frac{\partial \boldsymbol{\Lambda}^t}{\partial \boldsymbol{\sigma}} + \Delta\bar{\epsilon}^p \frac{\partial \boldsymbol{\Lambda}^p}{\partial \boldsymbol{\sigma}}$$

$$OC_2 = \Delta \boldsymbol{S}\boldsymbol{\sigma} + \Delta\boldsymbol{\alpha}\Delta T + \boldsymbol{\Lambda^t}$$

$$OC_3 = \boldsymbol{\Lambda}^p$$

$$A_1 = \frac{\dfrac{\partial \Phi^t}{\partial \boldsymbol{\sigma}}}{\dfrac{\partial \Phi^t}{\partial \xi}}$$

$$A_2 = \frac{\dfrac{\partial \Phi^p}{\partial \boldsymbol{\sigma}}}{\dfrac{\partial \Phi^p}{\partial \bar{\epsilon}^p}} - \frac{\dfrac{\partial \Phi^p}{\partial \xi}}{\dfrac{\partial \Phi^p}{\partial \bar{\epsilon}^p}} \frac{\dfrac{\partial \Phi^t}{\partial \boldsymbol{\sigma}}}{\dfrac{\partial \Phi^t}{\partial \xi}}$$

$$A_3 = \frac{\dfrac{\partial \Phi^t}{\partial T}}{\dfrac{\partial \Phi^t}{\partial \xi}}$$

$$A_4 = \frac{\dfrac{\partial \Phi^p}{\partial \xi}}{\dfrac{\partial \Phi^p}{\partial \bar{\epsilon}^p}} \frac{\dfrac{\partial \Phi^t}{\partial T}}{\dfrac{\partial \Phi^t}{\partial \xi}}$$

as a result,

$$\frac{d\boldsymbol{\sigma}}{d\boldsymbol{\epsilon}} = (OC_1 - OC_2 A_1 - OC_3 A_2)^{-1} \tag{3.44}$$

and

$$\frac{d\boldsymbol{\sigma}}{dT} = -(OC_1 - OC_2 A_1 - OC_3 A_2)^{-1}(\boldsymbol{\alpha} - OC_2 A_3 + OC_3 A_4) \tag{3.45}$$

The obtained Equations 3.44 and 3.45 are valid for transformation and yielding occurrence simultaneously. In case of a absence of one or two of these phenomena, the equations are modified accordingly. The terms related to $\Delta\xi$, $\Delta\bar{\epsilon}^p$ and $\Delta T$ drops, when there is no transformation, yielding or temperature change. ABAQUS global solver collects the data of Equations 3.44 and 3.45 in each increment for every node and comes up with a distributed result for each element.

# CHAPTER 4

# RESULTS AND DISCUSSION

## 4.1 Validation

In this section, the modified subroutine is validated by comparing the finite element results with the experimental and numerical results available in the literature. First, experimental results in the paper of Lagoudas [3] are used to validate the open source code [2] that represent the behaviour of SMA without plasticity. Second, the validation of the modified code including the generation of plastic strain is done by simple tension tests under various temperature and loading cases. The response of the material for each case is compared with the results of the paper of Hartl [4]. Finally, a three point bending test presented in the paper of Hartl [4] is simulated using the presented modified subroutine code. The resultant force displacement graphs at the contact point are compared.

### 4.1.1 The Verification of the Open Source Code

In this study, a SMA spring under large deformation is investigated. As the referenced paper suggests the stress generation while thermal induced actuation should be observed. A single-coiled helical spring with a coil diameter of 12.7 mm, wire diameter of 0.5 mm and pitch of 2.8 mm is used as the specimen. In order to represent the material behaviour, the properties of the nickel-rich NiTi are obtained from [3] and presented in Table 4.1.

The steps for thermomechanical loading are as follows. A force of 0.3 N is applied in the direction of expansion of the coil at 120 °C. While the load is maintained the

Table 4.1: Material Properties of nickel-rich NiTi for Spring Test

| $\rho(kg/m^3)$ | $E^A(GPa)$ | $E^M(GPa)$ | $\nu^A$ | $\nu^M$ | $\alpha(K^{-1})$ | $H_{sat}$ |
|---|---|---|---|---|---|---|
| 6500 | 90 | 63 | 0.3 | 0.3 | $10^{-5}$ | 0.016 |
| $k_t(Pa^{-1})$ | $\sigma_{cal}(MPa)$ | $T_{cal}(K)$ | $C^A(MPaK^{-1})$ | $C^M(MPaK^{-1})$ | $M_s(K)$ | $M_f(K)$ |
| $0.75.10^{-8}$ | 150 | 300 | 16 | 10 | 308 | 242 |
| $A_s(K)$ | $A_f(K)$ | $n_1$ | $n_2$ | $n_3$ | $n_4$ | $\phi_{tol}$ |
| 288 | 342 | 0.6 | 0.2 | 0.2 | 0.3 | $10^{-6}$ |
| $R_{tol}$ | | | | | | |
| $10^{-9}$ | | | | | | |

temperature is reduced to -30 °C and rised again to 120 °C. In the analysis of open source code, one end of the spring is assumed to be fixed and a force of 0.3 N applied to the other end only for simplicity. Deformed spring and stress distribution over a cross section which have been given in the reference [3] are shown in Figure 4.1 and Figure 4.2 respectively.

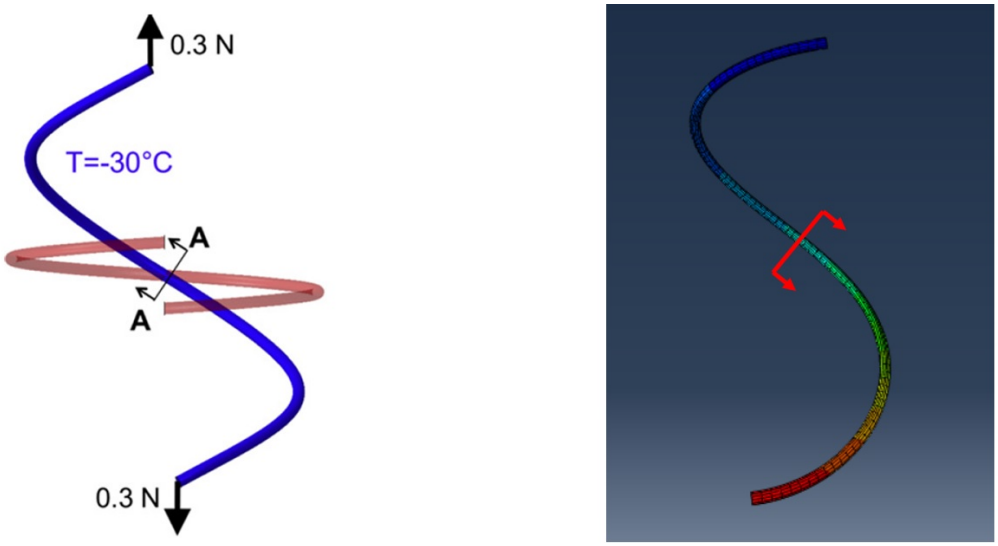


Figure 4.1: Spring under loading

Figure 4.3 shows the comparison of vertical deflection of the spring with respect to temperature obtained by the current study and reference [3]. As can be seen from the curve, for both cases the force first directly causes spring to deflect. With the

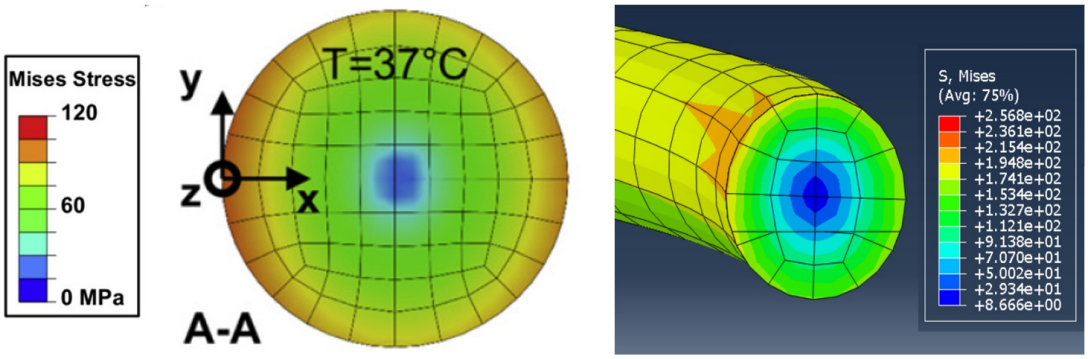


Figure 4.2: The stress distribution at 37 °C according to referenced paper [3] (Left) and resultant stress distribution of open source code at 37 °C (Right)

introduction of cooling, the primarily austenite SMA, transformed into martensite resulting in an excessive deformation. At the end of the cooling stage, the deflection has increased. Then, heating material to 120 °C has brought the material back to initial position without any strain residual. By that, both of the superelasticity and the shape memory effect of SMA are validated.

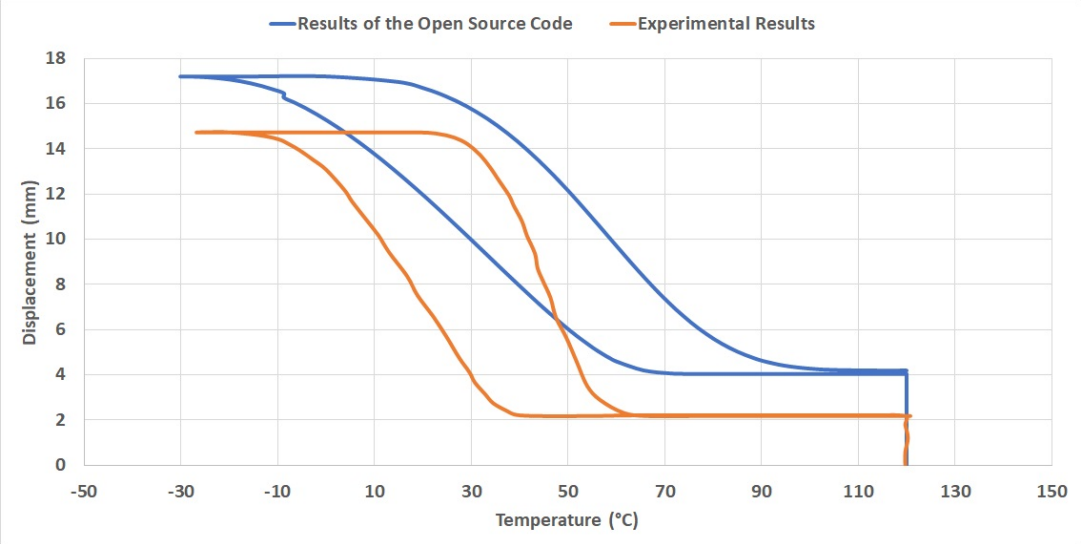


Figure 4.3: The deflection of the spring (left), the resultant displacement temperature curve of the node at the end (upper right), the stress distribution on the center (lower right)

When the graphs in Figure 4.3 are compared, it can be said that the conformity of the displacement obtained are reasonable and the Finite Element code is working

with slight deviation. There is 2 mm difference between the referenced paper and the code at each step. Also Figure 4.2 shows that, for analysis, the middle section has a very low stress while it keeps increasing towards the edge. There is small region that observed around 150 MPa while for rest of the outer region mainly is around 130 MPa. The results of referenced paper shows a maximum of 120 MPa for same region.

### 4.1.2 The Verification of the Modified Code via Simple Tension Test

After the subroutine code is validated as described in the previous section, the experimental results given in the study of Hartl [4] are used to show the effect of plasticity. The experiments were made on cold rolled, heat treated and quenched NiTi material and its properties are given in Table 4.2 [4]. For the sake of the verification of the proposed code, three of the experiments where the material is initially fully austenite, are taken into consideration. To compare the experimental results with the proposed model results, a 3D finite element model under uniaxial tension is constructed. The related loadings are applied to the part as the first step and unloading, are done at the second step. The resultant stress strain curves in combination with experimental results of these three experiments are given in Figures 4.4, 4.5 and 4.6 respectively.


Figure 4.4: The comparison of experimental and analysis results at 110 °C

As can be seen from the results in figures, the general behaviour of the material that are obtained by analyse is matching with the experimental data. However, as the

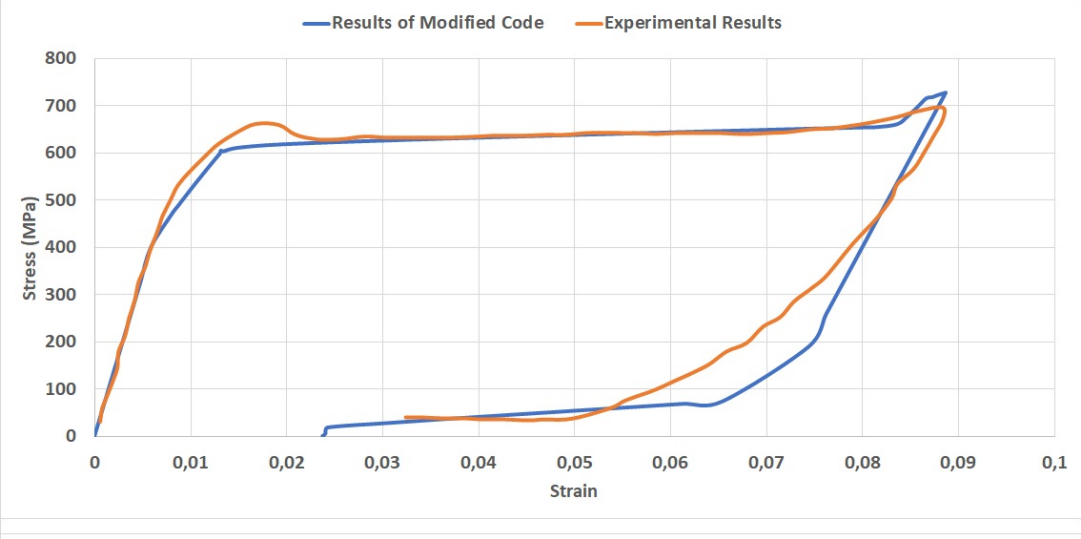


Figure 4.5: The comparison of experimental and analysis results at 120 °C

temperature increases, the residual strain starts to deviate from experimental results. Figure 4.4 and 4.5 show that, at 110 °C and 120 °C the residual strain are around 0.02 which is similar to experimental data. On the other hand, in Figure 4.6 at 140 °C the residual strain is found as 0.04 mm/mm while the experiments shows that it is around 0.06 mm/mm.

### 4.1.3 The Verification of the Modified Code via Three Point Bending Test

Lastly, a three point bending test is generated in ABAQUS framework in order to compare the proposed code in this thesis with the one that Hartl [4] worked in his paper. As the paper suggest, a 3D analysis of a dogbone specimen is subjected to a three point bending test under high temperature. The thermomechanical loading causes the material to undergo both transformation and plastic yielding. The same material properties in the simple tension test is used in the three point bending test [Table 4.2].

The loading is done under 133 °C temperature which above the austenite finish temperature meaning that the material is fully austenite. Two bars as encastered support and a bar for bending tip is used. The bars are modeled as rigid surfaces and the friction coefficient between the bars and the dogbone specimen is taken as 0.3. The

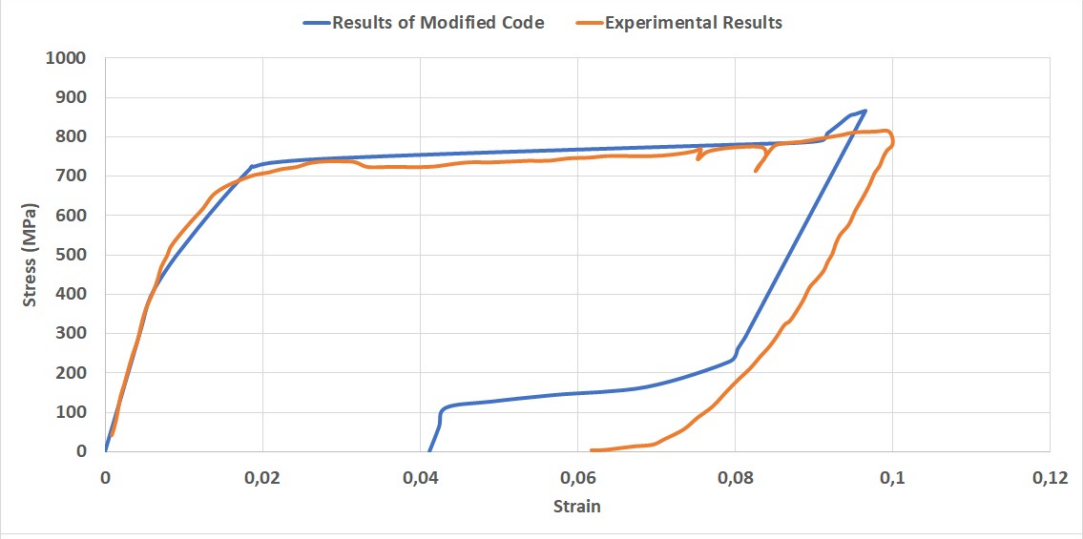


Figure 4.6: The comparison of experimental and analysis results at 140 °C

bending tip is moved 4.0 mm towards the supports and back to its original position in order to simulate the loading and unloading. The test, along with effective plastic strain distribution at a specific position are shown in Figure 4.7. The variation of the reaction force on the bending tip with respect to the deflection of the dogbone specimen curve obtained by the proposed model is compared with the experimental results in Figure 4.8.

According to the figures, it can be clearly seen that in both experiment and proposed model, the calculated residual effective plastic strain at the end of the unloadings are very close. While the experiment shows a 0.04 mm/mm plastic strain, the proposed model comes up with 0.037 mm/mm. However, the obtained reaction forces on the bending tip in both experiment and proposed model are slightly different than each other, at maximum deflection, 160 N and 188 N respectively.

## 4.2 Interpretation of the Results

In this section, the results obtained from the studies that are described in previous sections will be discussed thoroughly.

In the spring test, although the geometry is rather complex, the force and displacement

Table 4.2: Material Properties of NiTi for Simple Tension and Three Point Bending Tests

| $\rho(kg/m^3)$ | $E^A(GPa)$ | $E^M(GPa)$ | $\nu^A$ | $\nu^M$ | $\alpha(K^{-1})$ | $H_{sat}$ |
|---|---|---|---|---|---|---|
| 6500 | 69 | 38 | 0.33 | 0.33 | $10^{-6}$ | 0.06 |
| $k_t(Pa^{-1})$ | $\sigma_{cal}(MPa)$ | $T_{cal}(K)$ | $C^A(MPaK^{-1})$ | $C^M(MPaK^{-1})$ | $M_s(K)$ | $M_f(K)$ |
| $1.29.10^{-8}$ | 150 | 300 | 7 | 8.7 | 321 | 319 |
| $A_s(K)$ | $A_f(K)$ | $n_1$ | $n_2$ | $n_3$ | $n_4$ | $\phi_{tol}$ |
| 373 | 380 | 0.95 | 0.95 | 0.95 | 0.95 | $10^{-6}$ |
| $R_{tol}$ | $Y_0^A(MPa)$ | $Y_0^M(MPa)$ | $Y_M^A(MPa)$ | $Y_M^A(MPa)$ | $C_H$ | $K_\beta^A(GPa)$ |
| $10^{-9}$ | 420 | 500 | 1000 | 1050 | 80 | 11.3 |
| $K_\beta^M(GPa)$ | $\epsilon_{crit}$ | | | | | |
| 8.3 | 0.022 | | | | | |

relation has shown similarity with the experimental results shown in the reference paper [3]. The calculated initial jump is 4 mm while the value found by reference [3] is around 3 mm. The difference is kept constant while the part transforms, and the loops in the graphs of the proposed model and the reference [3] reach 15 mm and 16 mm respectively. Additionally, the stress level at 37 °C differs slightly. In the referenced paper, the cross section has around 60 MPa Misses stress in general. However in the analysis, the von Mises stress is around 80 MPa.

The obtained deviations in the analysis are attributed to the lack of proper material properties. The open source code is working with 38 input data that include the initial direction of the transformation, effective specific heat, density, calibration stress, calibration temperature and the most importantly model parameters. All of these properties are not provided for the analysis in the papers. Therefore, commercially available data for missing properties are used. Considering their effect on the constitutive equations, the deviation of the stress and displacement that occur can be explained.

In the case of simple tension test, the experimental values in Figures 4.4, 4.5 and 4.6 show that under 600 MPa, 700 MPa and 800 MPa, the material streches up to 8%, 9% and 10% respectively. When the material is unloaded, the resultant residual plastic

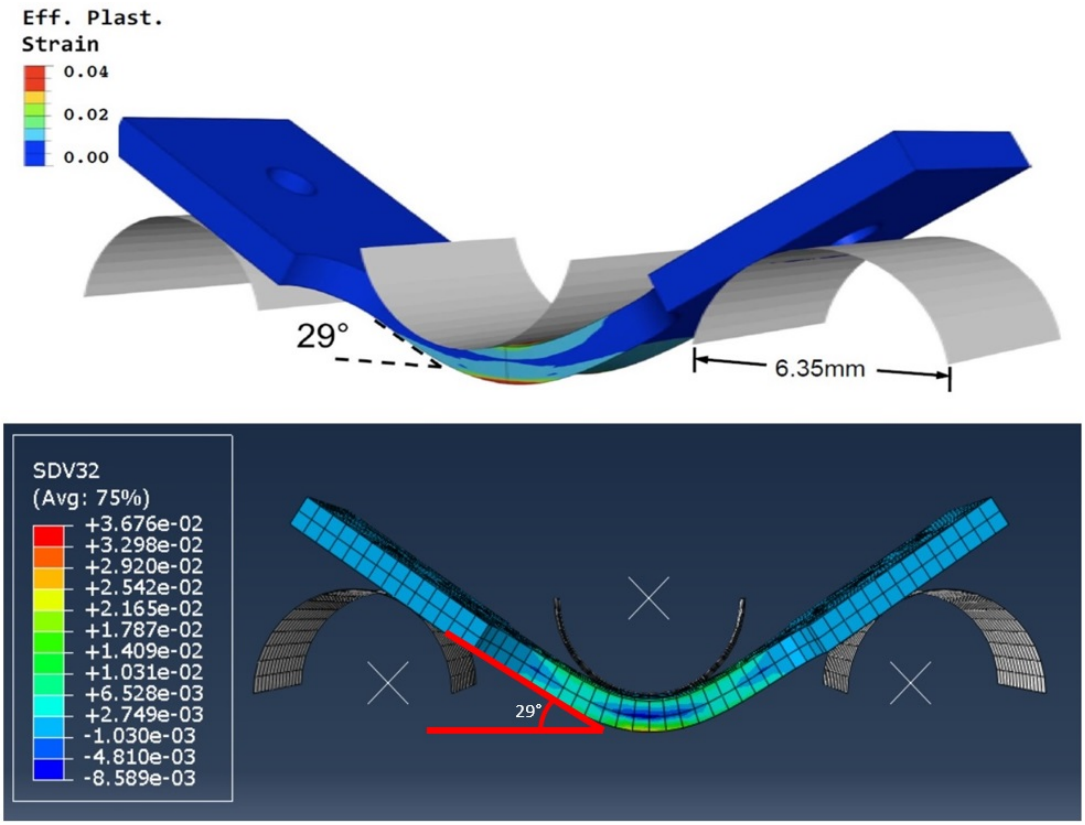


Figure 4.7: Analysis results of referenced paper [4] (Upper) and analysis results of modified code (Lower)

strains are as follows: 2.5%, 3.5% and 6.5% . When the proposed code in this thesis is run under the same conditions, as Figures 4.4, 4.5 and 4.6 show, 600 MPa, 700 MPa and 800 MPa have streched the specimen around 8%, 9% and 10% while the resultant plastic strains are observed to be 2%, 2.5% and 4%.

For all of the simple tension cases, when the stress reaches around 450 MPa, the yielding in austenite phase starts with linear hardening. This yielding behaviour at austenite phase is unique to study of Hartl [4] and expected as described in the literature survey chapter. For each temperature, transformation starts at different stress level and transformation strain occurs within a short stress increase. Up to that point, the model shows considerable similarity with the literature. However, at 120 °C and 140 °C, the completion of the transformation is obtained earlier than reported in the literature resulting in a peak. This peak is caused from yielding at martensite phase. It is observed that due to fully martensitic transformation and hardening at marten-

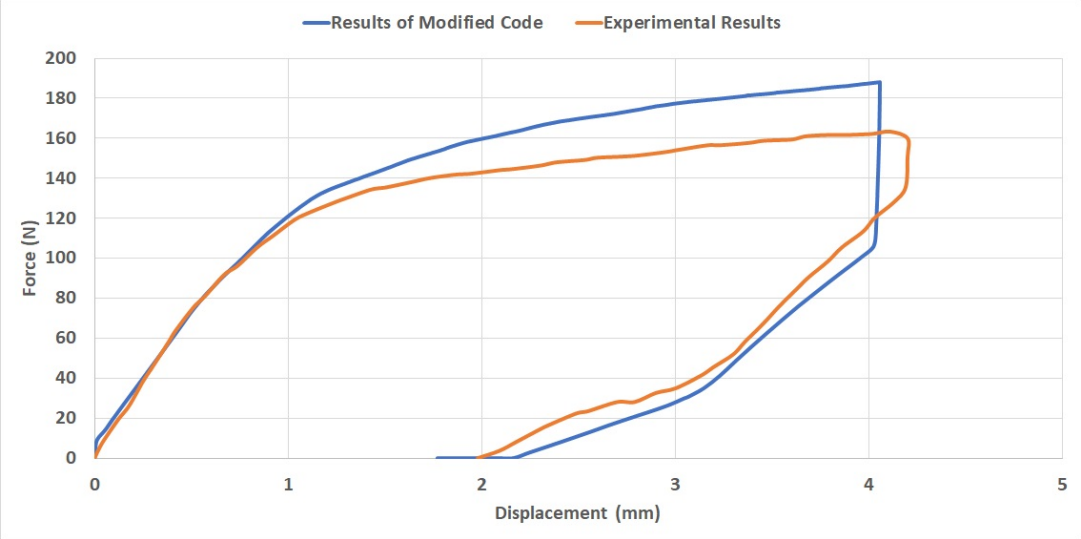


Figure 4.8: The force deflection curve comparison

sitic phase, the residual strain build up observed at the end of the simulation differs significantly for higher temperatures from the experimental values.

For the three point bending test, the experimental data in Figure 4.8 shows 4 mm deflection under 160 N force. This loading results in 4% plastic strain after unloading. Similar to the simple tension test, three point bending test is conducted at 133 °C which means that the phase of the material is full austenite. Therefore this test also considers the effect of superelasticity in combination with plasticity. When the same properties at same conditions applied to the same specimen the outcome of the proposed code is as Figures 4.7 and 4.8 show. The force versus displacement curves differ slightly. Instead of 160 N, the specimen reaches the same deformation value at 188 N in the proposed analysis. At the maximum deformation point, the observed strain is 3.7% while the paper suggests 4%.

The residual strain at the end of the three point bending test fits well with the literature. Apart from simple tension test, an initial displacement is given instead of applying stress directly. Although the residual strain is similar to the one obtained in the experiment, the reaction force obtained from the bending tip differs. In addition to lack of material properties, the Newton-Rhapson method may have an impact on this difference.

As a general fact, the newly generated code has stability issues which may be due to the number of iterations of Newton-Rhapson method in each increment for every element. Currently, the code checking the transformation function and plastic yield function at each step. If any one of them or both of them are larger than zero, the code starts to calculate transformation strain and platic strain simultaneously and repeatedly via Newton-Rhapson method until it finds a result suitable for given tolerances. Therefore a large amount of iteration might be required for some steps which might result in abortion of the analysis.

# CHAPTER 5

# CONCLUSIONS AND FUTURE WORK

## 5.1 Conclusions

The present study, starting from the basic characteristics, evaluates the constitutive relations, the effect of plasticity and finally numerical implementation of the constitutive equations of SMA. According to the results obtained, following conclusions are made:

1. The implementation of the user subroutine for modelling of the shape memory effect, superelastic and plastic behaviour via Newton-Rhapson method gives results that match considerably with the studies that are modelling SMA using convex cutting plane algorithm. In the validation studies; the shape memory effect is shown in spring test, simple tension tests and three point bending test show the combination of superelastic and plastic behaviour and overall promising results are obtained.

2. Experimentally obtained model parameters have an impact on the behaviour of the material. This deviation is attributed consequence of lack of model parameters which are replaced by commercially available data. This assumption has also affected simple tension and three point bending tests.

3. In the simple tension test, the proposed code of SMA including plasticity has shown a good match with referenced paper [4] in terms of plasticity in the austenitic phase and transformation. The yielding and hardening at the austenite phase is a unique to that paper. Similar studies in the literature, does not include the austenitic yielding and hardening in the constitutive modelling.

4. In the simple tension test, under tension, the material has transformed into fully martensite phase at 120 °C and 140 °C. For both cases, the transformation starts around 420 MPa and ends around 750 MPa and 850 MPa, respectively and the end of the transformation, results in a peak in stress strain diagram due to yielding at martensite phase, in the proposed code.

5. For three point bending test, with the proposed code residual strains are obtained close to literature values. Comparing with the simple tension test, applying initial displacement instead of stress, results in better solutions.

6. As result, the modelling of SMA through a user subroutine that includes plasticity in the finite element tool is realized. The implementation of the user subroutine using Newton-Rhapson is found to be sufficient to model the plastic response.

## 5.2 Future Work

The model parameters and other missing material properties can be replaced by the exact ones. Experiments will be needed to collect the missing information. This will lead to a better simulation. New physical experiments can be conducted in order to obtain the shape memory effect in combination with plasticity. The current code needs optimization with the obtained results.

Finally, the Newton-Rhapson method used in the coding can be optimized in order to enhance the capability and stability of the code.

# REFERENCES


[1] D. C. Lagoudas, *Shape memory alloys: modeling and engineering applications*. Springer, 2008.

[2] A. Karakalas, "Thermomechanically coupled analysis and experimental investigation of morphing structures with shape memory alloy actuators operating under partial transformation with a focus on active load control," *Unviersity of Patras*, 2019.

[3] D. Lagoudas, D. Hartl, Y. Chemisky, L. Machado, and P. Popov, "Constitutive model for the numerical analysis of phase transformation in polycrystalline shape memory alloys," *International Journal of Plasticity*, vol. 32, pp. 155–183, 2012.

[4] D. Hartl and D. Lagoudas, "Constitutive modeling and structural analysis considering simultaneous phase transformation and plastic yield in shape memory alloys," *Smart Materials and Structures*, vol. 18, no. 10, p. 104017, 2009.

[5] K. Otsuka and C. M. Wayman, *Shape memory materials*. Cambridge university press, 1999.

[6] P. Rodriguez and G. Guénin, "Stability of the two way memory effect during thermal cycling of a high ms temperature cu-al-ni alloy," in *Materials Science Forum*, vol. 56, pp. 541–546, Trans Tech Publ, 1990.

[7] N. Liu and W. Huang, "Dsc study on temperature memory effect of niti shape memory alloy," *Transactions of Nonferrous Metals Society of China*, vol. 16, pp. s37–s41, 2006.

[8] J. A. Shaw *et al.*, "Tips and tricks for characterizing shape memory alloy wire: part 1—differential scanning calorimetry and basic phenomena," 2008.

[9] B. D. Coleman and M. E. Gurtin, "Thermodynamics with internal state variables," *The journal of chemical physics*, vol. 47, no. 2, pp. 597–613, 1967.

[10] L. Machado and D. Lagoudas, "Thermomechanical constitutive modeling of smas," in *Shape Memory Alloys*, pp. 121–187, Springer, 2008.

[11] C. Liang and C. Rogers, "A multi-dimensional constitutive model for shape memory alloys," *Journal of Engineering Mathematics*, vol. 26, no. 3, pp. 429–443, 1992.

[12] D. Lagoudas, Z. Bo, M. Qidwai, and P. Entchev, "Sma um: user material subroutine for thermomechanical constitutive model of shape memory alloys," *Texas A&M University College Station TX*, 2003.

[13] W. Buehler and R. Wiley, "The properties of tini and associated phases," tech. rep., Naval Ordnance Laboratoy, 1961.

[14] W. J. Buehler, J. V. Gilfrich, and R. Wiley, "Effect of low-temperature phase changes on the mechanical properties of alloys near composition tini," *Journal of applied physics*, vol. 34, no. 5, pp. 1475–1477, 1963.

[15] J. Perkins, *Shape memory effects in alloys*. Springer Science & Business Media, 2012.

[16] H. Funakubo and J. Kennedy, "Shape memory alloys," *Gordon and Breach, xii+ 275, 15 x 22 cm, Illustrated*, 1987.

[17] J. N. Kudva, "Overview of the darpa smart wing project," *Journal of intelligent material systems and structures*, vol. 15, no. 4, pp. 261–267, 2004.

[18] T. Duerig, A. Pelton, and D. Stöckel, "An overview of nitinol medical applications," *Materials Science and Engineering: A*, vol. 273, pp. 149–160, 1999.

[19] R. W. Gaines Jr, "The use of pedicle-screw internal fixation for the operative treatment of spinal disorders," *JBJS*, vol. 82, no. 10, p. 1458, 2000.

[20] H. Prahlad and I. Chopra, "Design of a variable twist tilt-rotor blade using shape memory alloy (sma) actuators," in *Smart Structures and Materials 2001: Smart Structures and Integrated Systems*, vol. 4327, pp. 46–59, SPIE, 2001.

[21] B. Santoni, R. Hynes, K. McGilvray, G. Rodriguez-Canessa, A. Lyons, M. Henson, W. Womack, and C. Puttlitz, "Cortical bone trajectory for lumbar pedicle screws," *The Spine Journal*, vol. 9, no. 5, pp. 366–373, 2009.

[22] *ASTM International, Standard Test Method for Tension Testing of Nickel-Titanium Superelastic Materials (2006).*

[23] *ASTM International, Standard Test Method for Transformation Temperature of Nickel-Titanium Alloys by Thermal Analysis (2005).*

[24] J. Lemke and A. Coda, "Dsc and microstructure analysis of high temperature ni-ti-hf, low hysteresis ni-ti-cu and conventional super-elastic and shape memory ni-ti alloy ingots and wires," *Materials Today Communications*, vol. 21, p. 100666, 2019.

[25] N. Farjam, M. Nematollahi, M. T. Andani, M. J. Mahtabi, and M. Elahinia, "Effects of size and geometry on the thermomechanical properties of additively manufactured niti shape memory alloy," *The International Journal of Advanced Manufacturing Technology*, vol. 107, no. 7, pp. 3145–3154, 2020.

[26] *ASTM International, Standard Test Methods of Compression Testing of Metallic Materials at Room Temperature (2000).*

[27] H. Sehitoglu, I. Karaman, R. Anderson, X. Zhang, K. Gall, H. Maier, and Y. Chumlyakov, "Compressive response of niti single crystals," *Acta Materialia*, vol. 48, no. 13, pp. 3311–3326, 2000.

[28] D. A. Miller and D. C. Lagoudas, "Thermomechanical characterization of niticu and niti sma actuators: influence of plastic strains," *Smart Materials and Structures*, vol. 9, no. 5, p. 640, 2000.

[29] T. Hu and C. S. Wen, "Wear resistance of niti alloy after surface mechanical attrition treatment," *Surface and Coatings Technology*, vol. 205, no. 2, pp. 506–510, 2010.

[30] "Surface characteristics and corrosion resistance properties of tini shape memory alloy coated with ta," *Surface and Coatings Technology*, vol. 186, no. 3, pp. 346–352, 2004.

[31] K. Tanaka, "A thermomechanical sketch of shape memory effect: one-dimensional tensile behavior," *Res. Mechanica*, vol. 18, pp. 251–263, 1986.

[32] C. Liang and C. A. Rogers, "One-dimensional thermomechanical constitutive relations for shape memory materials," *Journal of intelligent material systems and structures*, vol. 8, no. 4, pp. 285–302, 1997.

[33] L. C. Brinson, "One-dimensional constitutive behavior of shape memory alloys: thermomechanical derivation with non-constant material functions and redefined martensite internal variable," *Journal of intelligent material systems and structures*, vol. 4, no. 2, pp. 229–242, 1993.

[34] F. Auricchio and E. Sacco, "A one-dimensional model for superelastic shape-memory alloys with different elastic properties between austenite and martensite," *International Journal of Non-Linear Mechanics*, vol. 32, no. 6, pp. 1101–1114, 1997.

[35] S. Govindjee and E. P. Kasper, "Computational aspects of one-dimensional shape memory alloy modeling with phase diagrams," *Computer Methods in Applied Mechanics and Engineering*, vol. 171, no. 3, pp. 309–326, 1999.

[36] A. Paiva and M. A. Savi, "A constitutive model for shape memory alloys considering tensile–compressive asymmetry and plasticity," *International Journal of Solids and Structures*, vol. 42, no. 11, pp. 3439–3457, 2005.

[37] M. Savi and A. Paiva, "Describing internal subloops due to incomplete phase transformations in shape memory alloys," *Archive of Applied Mechanics*, vol. 74, no. 9, pp. 637–647, 2005.

[38] A. P. Baêta-Neves, M. A. Savi, and P. M. Pacheco, "On the fremond's constitutive model for shape memory alloys," *Mechanics Research Communications*, vol. 31, no. 6, pp. 677–688, 2004.

[39] J. G. Boyd and D. C. Lagoudas, "A thermodynamical constitutive model for shape memory materials. part i. the monolithic shape memory alloy," *International Journal of Plasticity*, vol. 12, no. 6, pp. 805–842, 1996.

[40] J. G. Boyd and D. C. Lagoudas, "A thermodynamical constitutive model for shape memory materials. part ii. the sma composite material," *International Journal of Plasticity*, vol. 12, no. 7, pp. 843–873, 1996.

[41] E. Patoor, A. Eberhardt, and M. Berveiller, "On micromechanics of thermoelastic phase transition," in *proceedings of Plasticity*, vol. 93, 1993.

[42] B. Raniecki and C. Lexcellent, "Rl-models of pseudoelasticity and their specification for some shape memory solids," *European journal of mechanics. A. Solids*, vol. 13, no. 1, pp. 21–50, 1994.

[43] D. C. Lagoudas, Z. Bo, and M. A. Qidwai, "A unified thermodynamic constitutive model for sma and finite element analysis of active metal matrix composites," *Mechanics of composite materials and structures*, vol. 3, no. 2, pp. 153–179, 1996.

[44] M. Qidwai and D. Lagoudas, "On thermomechanics and transformation surfaces of polycrystalline niti shape memory alloy material," *International journal of plasticity*, vol. 16, no. 10-11, pp. 1309–1343, 2000.

[45] L. Juhasz, E. Schnack, O. Hesebeck, and H. Andrä, "Macroscopic modeling of shape memory alloys under non-proportional thermo-mechanical loadings," *Journal of intelligent material systems and structures*, vol. 13, no. 12, pp. 825–836, 2002.

[46] D. C. Lagoudas and P. B. Entchev, "Modeling of transformation-induced plasticity and its effect on the behavior of porous shape memory alloys. part i: constitutive model for fully dense smas," *Mechanics of Materials*, vol. 36, no. 9, pp. 865–892, 2004.

[47] P. B. Entchev and D. C. Lagoudas, "Modeling of transformation-induced plasticity and its effect on the behavior of porous shape memory alloys. part ii: porous sma response," *Mechanics of Materials*, vol. 36, no. 9, pp. 893–913, 2004.

[48] X. Wang, B. Xu, and Z. Yue, "Phase transformation behavior of pseudoelastic niti shape memory alloys under large strain," *Journal of Alloys and Compounds*, vol. 463, no. 1, pp. 417–422, 2008.

[49] C. M. L. Dongjie Jiang, "A constitutive model for isothermal pseudoelasticity coupled with plasticity," *Shape Memory and Superelasticity*.

[50] A. Zou, Y. Wang, and Q. Zhang, "Constitutive model of shape memory alloy under the effect of martensite plasticity for finite-element applications," *The Journal of Engineering*, vol. 2019, no. 13, pp. 424–426, 2019.

[51] G. Scalet, F. Niccoli, C. Garion, P. Chiggiato, C. Maletta, and F. Auricchio, "A three-dimensional phenomenological model for shape memory alloys including two-way shape memory effect and plasticity," *Mechanics of Materials*, vol. 136, p. 103085, 2019.

[52] L. Petrini and A. Bertini, "A three-dimensional phenomenological model describing cyclic behavior of shape memory alloys," *International Journal of Plasticity*, vol. 125, pp. 348–373, 2020.

[53] A. S. Khan and S. Huang, *Continuum theory of plasticity*. John Wiley & Sons, 1995.

[54] F. Abaqus *et al.*, "Abaqus analysis user's manual," *Dassault Systemes, Vélizy-Villacoublay, France*, 2009.